(29)

Enhanced Performance Of

A Low Noise Discrete

Pre-Amplifier Stage

by

Akin Adeniyi Aina

Submitted to the Department of Electrical Engineering and Computer Science in Partial Fulfillment of the Requirements for the Degrees of Bachelor of Science
and
Masters of Engineering in Electrical Engineering
at the MASSACHUSETTS INSTITUTE OF TECHNOLOGY
May 23, 1997

Author ....
Department of Electrical Engineering
May 23, 1997

Certified by .....
Doctor Chathan M. Cooke
Thesis Supervisor

Accepted by .....
E. R. Morgenthaler
Chairman, Department Committee on Graduate Theses

Enhanced Performance Of

A Low Noise Discrete

Pre-Amplifier Stage

by

Akin A. Aina

Submitted to the Department of Electrical Engineering and Computer Science in Fulfillment of the Requirements for the Degree of Bachelor of Science in Electrical Engineering & Computer Science and for the Masters of Engineering Degree in Electrical Engineering and Computer Science at the Massachusetts Institute of Technology

ABSTRACT

This paper contains the modeling of a bipolar transistor's noise sources and the derivation of the minimum detectable signal (MDS) as the sum of thermal and shot noise. The MDS is used to measure the noise performance of a circuit because it lends itself to understanding which noise generators dominate the noise performance.

This paper discusses the fundamentals of noise theory and illustrates the effects of the design parameters on the minimum detectable signal and the more commonly used measure of noise performance, noise figure. It presents which parameters have the most prominent effect on the noise performance and how to design such low noise amplifiers.

Thesis Supervisor: Doctor Chathan Cooke
Title: Principal Research Engineer

TABLE OF CONTENTS

List of Figures

List of Tables

Chapter 1

INTRODUCTION TO LOW NOISE THEORY

1.1 The Noise Problem

Sensors, detectors, and transducers measure characteristics of the real world. Their measurements are converted into weak electrical signals that have to be amplified before they are processed. During the measurement process, the sensor adds unwanted noise to the signal. This leaves the engineer with the task of designing an amplifier that will maximize the signal level while contributing a minimum amount of noise.

Noise in semiconductor amplifiers is a problem because it degrades the signal-to-noise ratio as it amplifies its input. This noise is often denoted by a quantity known as the "noise figure", expressed in decibels (dB). However, this quantity does not lend itself as a straightforward approach to optimizing the "Optimum Low-Noise Amplifier" problem.

To better understand the needed tradeoffs and design issues, this paper includes a more exhaustive analysis via the minimum detectable signal. This approach facilitates the analysis of noise contributions to signals in semiconductor amplifiers, specifically with bipolar junction transistors.

1.2 Measures of Noise Performance

The most important issue in this design is noise. Noise can be defined as any unwanted disturbance that obscures or interferes with a signal (Motchenbacher & Fitchen, p. 7). Noise in a transistor amplifier can be quantified by its minimum detectable signal or its noise figure.

1.2.1 Minimum Detectable Signal

This paper is concerned with optimizing the noise performance of a transistor amplifier. The significance of noise performance of an amplifier is the limit it places on the smallest input signals that it can amplify before its noise degrades the quality of the output. The noise performance is usually expressed in terms of an equivalent input noise signal, which when applied to an identical but noiseless amplifier, gives the same output noise as the noisy circuit. This way, the equivalent input noise can be compared to incoming signals and the effect of the noise on input signals can be easily determined (Gray & Meyer, pp. 735-6).

The equivalent input noise is found by calculating the total rms output voltage of the circuit with no input, and dividing it by the amplifier gain. If no special filtering or coding techniques are used, the minimum detectable signal is equal to the equivalent input noise voltage within the passband of the amplifier (Gray & Meyer, p. 737).

1.2.2 Noise Figure vs. MDS

A traditional figure of merit for an amplifier with respect to noise is its "noise figure", also known as the noise factor. According to IEEE standards, the noise factor of a device is the ratio of the available output noise power per unit bandwidth to the portion of that noise caused by the actual source connected to the input terminals of the device, measured at the standard temperature of 290°K (Motchenbacher & Fitchen, p. 34).

Another definition of the noise figure is the signal to noise power ratio at the amplifier input divided by the corresponding ratio at the output. This can be expressed is decibels (dB) as

$$NF = 10 \log_{10}\left(\frac{(S/N)_{IN}}{(S/N)_{OUT}}\right).$$

This approach to noise analysis indicates that decreasing the noise at the output improves the noise figure of a noisy amplifier, although it does not provide any insight as to how to actually achieve the noise reduction.

On the other hand, the minimum detectable signal (MDS) approach offers a detailed analysis of all noise sources and the circuit topology to establish the total noise on a component by component basis. This facilitates a more detailed prediction of the noise performance of the circuit.

1.3 Project Goals

This thesis is concerned with understanding the sources of noise in bipolar junction transistor amplifiers. Also, the factors that influence the minimum detectable signal and noise figure will be identified so that a

circuit designer can optimize a transistor amplifier design for the minimum detectable signal. In this paper, three preamplifier designs will be discussed as examples of low-noise methodologies. The preamplifier's role is to raise the signal level with minimal additional noise so that when connected to a low noise operational amplifier, such as National Semiconductor's CLC425[1], optimum overall noise performance is achieved.

[1] The CLC425 has a 1.9 GHz gain-bandwidth product, 1 nV/√Hz, and 1 pA/√Hz

Chapter 2

BIPOLAR JUNCTION TRANSISTOR NOISE FUNDAMENTALS

Noise is present in all semiconductor devices. It exists due to Brownian motion of carriers in conductors, generation and recombination of carriers in the surfaces of semiconductors and the fact that a dc current is not continuous, but rather the sum of pulses of current.

This chapter briefly discusses noise theory, and relates the theory to the noise sources in the bipolar junction transistor noise model.

2.1 Noise Theory

There are three main types of noise mechanisms: thermal noise, shot noise and flicker (1/*f*) noise. All of these are found in transistors and they are associated with physical processes in materials.

2.1.1 Thermal Noise

Thermal noise is due to the random thermal excitation of electrons in semiconductors at all temperatures above absolute zero. This excitation, similar to Brownian motion of particles, is dependent on temperature. Since each electron carries a charge of 1.6×10^{-19} C, there are small current surges in the material generated when the electrons move. Although the

average current that results from these transitions is zero, there is an instantaneous current that will generate a voltage across the terminals of the conductor (Motchenbacher & Fitchen, p. 10).

The amplitude of the noise voltage can range from very small to very large values and its exact value at any moment in time cannot be predicted. Therefore, thermal noise cannot be measured as peak voltages and its root-mean-square (rms) value is used to quantify it. The open-circuit thermal noise voltage of a resistor is given by

$$E_{th}^2 = 4kTR$$

where E_{th}^2 is in units of Volts squared per Hertz, k is Boltzman's constant, T is the absolute temperature in degrees Kelvin and R is the value of the resistor in Ohms (Hardy, p. 2). The above thermal noise density is constant up to infrared frequencies, where quantum effects cause it to drop (Lundberg, p. 10).

Resistors made from composition carbon also exhibit a phenomenon known as excess noise, in addition to thermal noise, when a dc current is present. Excess noise arises from the fact that current does not flow evenly in a carbon resistor and exhibits a $1/f$ noise spectrum. This makes carbon resistors unsuitable for use in low noise applications and instead, wirewound resistors, which usually do not exhibit a significant amount of excess noise, are a better choice (Motchenbacher & Fitchen, p. 18).

2.1.2 Shot Noise

Shot noise is present in vacuum tubes, diodes and transistors. It is due to the fact that current flowing in these devices is not smooth and continuous,

but it is the sum of pulses of current across a barrier such as the cathode surface in vacuum tubes and pn-junctions in diodes and bipolar transistors, caused by the flow of carriers, each carrying 1.6 x 10^{-19} C of charge (Motchenbacher & Fitchen, p. 21).

This pulsing flow is a granule effect, and the variations are the cause of shot noise (Lundberg, p. 10). The mean-square value of shot noise is observed to be given by

$$I_{sh}^2 = 2qI$$

where I_{sh}^2 has units of Amps squared per Hertz, q is the electronic charge, and I is the dc current flowing in the device (Motchenbacher & Fitchen, p. 21).

The expression above is valid in the useful frequency range of the device and up to frequencies close to $1/\tau$, where τ is the transit time through the barrier (Lundberg, p. 10).

2.1.3 Flicker Noise

The spectral density of $1/f$ or low frequency noise increases without bound as frequencies decrease. It has received the name flicker noise from the "flicker effect", which was the flickering effect observed in the plate current of vacuum tubes (Motchenbacher & Fitchen, p. 19). The major cause of $1/f$ noise in semiconductor devices can be found in the properties of the surface of the material. The generation and recombination of carriers in surface energy states and the density of these energy states are important factors. This occurs at interfaces between silicon surfaces and grown oxide

(Motchenbacher & Fitchen, p. 19). The mean square flicker noise in a device is

$$I_{fl}^2 = \frac{2qIf_L}{f}$$

where I_{fl}^2 has units of Amps squared per Hertz, q is the electron charge, I is the dc current flowing in the material, f is the frequency in Hertz, and f_L is a constant depending on the type of material and its geometry (Lundberg, p. 11). This constant can vary by orders of magnitude from one device to the next or it can vary widely for different transistors. Therefore, multiple measurements are made and an average f_L is computed then this value is used to predict an average or typical flicker noise performance for that device (Gray & Meyer, p. 722). Fortunately, current surface treatment in device manufacturing has decreased flicker noise to an insignificant level (Lundberg, p. 11).

2.1.4 Noise Bandwidth

Noise bandwidth is not the same as the 3-dB bandwidth that is more commonly used. The 3-dB bandwidth is defined as the frequency span between half-power points, while the noise bandwidth is the frequency span of a rectangularly shaped power gain curve equal in area to the area of the actual power gain versus frequency curve (Motchenbacher & Fitchen, p. 13). Since the power gain is proportional to the voltage gain squared, the noise bandwidth can be expressed as

$$\Delta f = \frac{1}{A_{vo}^2}\int_0^\infty \left|A_v(f)\right|^2 df$$

where A_v is the voltage gain as a function of frequency and A_{vo} is the midband voltage gain (Motchenbacher & Fitchen, p. 14).

Considering an amplifier with a single-pole frequency response given by

$$A_v(jf) = \frac{A_{vo}}{1 + j\frac{f}{f_{3dB}}}$$

where f_{3dB} is the 3-dB frequency, the noise bandwidth can be calculated as $1.57f_{3dB}$. In summary, a circuit with the above voltage gain will produce noise as if it had an abrupt band edge at $1.57f_{3dB}$ (Gray & Meyer, p. 770).

2.2 Noise Sources

In this section, the noise model and the noise sources in a bipolar junction transistor small signal model are presented.

2.2.1 Noise Model

The hybrid-pi model including its noise sources is shown below. They arise from separate, independent mechanisms, therefore the noise sources are independent of each other (Gray & Meyer, p. 726).

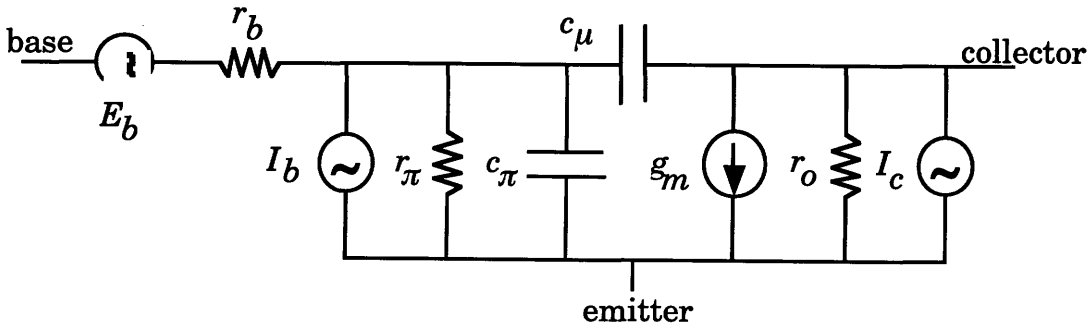

Figure 2-1: The hybrid-pi model of the bipolar transistor with noise sources

2.2.2 r_B Noise

The resistors r_π, and r_o are fictitious resistances that are used for modeling purposes. Therefore, they do not contribute any noise. However, the transistor base resistor, r_b is a physical resistor and as such it has thermal noise given by

$$E_b^2 = 4kTr_b$$

This is modeled as a voltage source of E_b in series with r_b.

2.2.3 I_b Noise

The base current, I_B, flows in a transistor due to recombination in the base and base-emitter depletion regions and also due to carrier injection into the base from the emitter. All of these processes are independent, therefore the base shows full shot noise. This is modeled as a current source in parallel with c_π and r_π with mean-squared value

$$I_b^2 = 2qI_B.$$

Also, flicker noise has been experimentally found in the base and in the noise model, it is a current source across the base and emitter terminals which can be combined with the shot noise generator I_b The flicker noise in the base is given by

$$I_f^2 = \frac{2qf_L I_B}{f}$$

in Amps squared per Hertz.

2.2.4 I_c Noise

When a bipolar transistor is biased for forward-active operation, minority carriers that enter the collector-base depletion region are swept into the collector by the field existing there. The arrival of the carriers at the collector-base junction is a random process, so the collector current is a result of the sum of the current pulses that result when each carrier crosses the region. For this reason, collector current exhibits shot noise, which is represented in the model as a current source in parallel with the output resistance, r_o, of the transistor. The mean squared collector current shot noise is

$$I_c^2 = 2qI_C$$

where I_C is the dc collector current.

2.3 Noise Components of the Minimum Detectable Signal

All of the noise components discussed in the previous sections can be added together to yield the minimum detectable signal (MDS) for a common-emitter topology. The MDS, as derived in Appendix B, can be expressed as

$$E_{mds}^2 = \frac{4kT}{R_1}Z_s^2 + \frac{4kT}{R_2}Z_s^2 + 4kTr_bZ_s^2G_s^2 + 2qI_BZ_s^2(G_sr_b+1)^2 +$$

$$2qI_cZ_s^2\left(\frac{(G_sr_b+1)\left(\frac{1}{z_\pi}+\frac{1}{z_\mu}\right)+G_s}{g_m-\frac{1}{z_\mu}}\right)^2 + \frac{4kT}{R_L}Z_s^2\left(\frac{(G_sr_b+1)\left(\frac{1}{z_\pi}+\frac{1}{z_\mu}\right)+G_s}{g_m-\frac{1}{z_\mu}}\right)^2$$

The input noise is the noise observed at the output terminals referred to the input by dividing the output noise by the amplifier gain. A plot of the input noise, the MDS and all of its components are plotted below for a noise bandwidth of 100 MHz, for the NE856 NPN device in a common emitter amplifier configuration.

100 MHz MDS & Its Components for the NE856

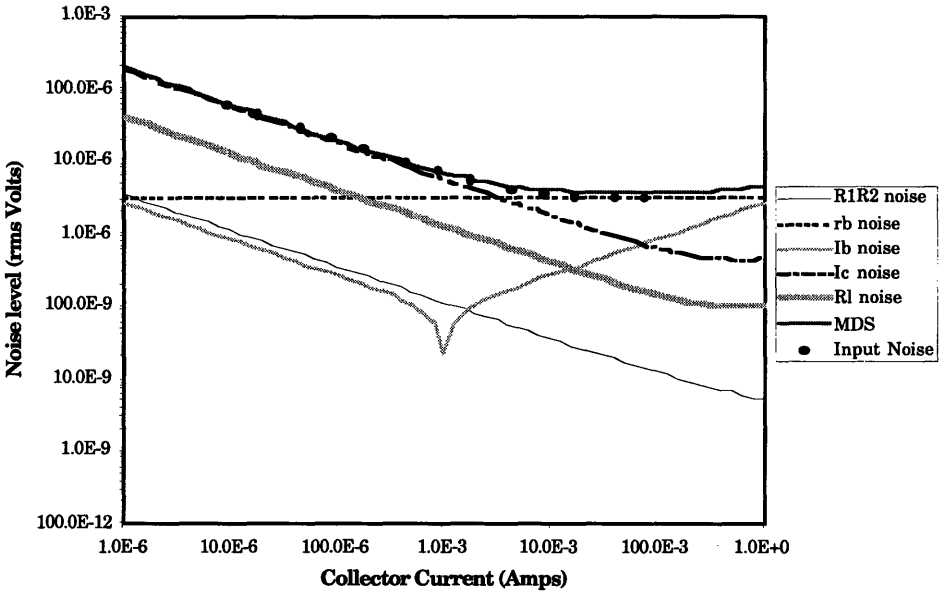

Figure 2-2: MDS & its noise components versus collector current

From the above plot, it is evident that there are three regions of noise performance, each dominated by a different noise contributor.

Region 1. At low currents, the MDS is dominated by collector current shot noise.

Region 2. The noise floor is set by the base resistance, r_b, and since r_b varies from transistor to transistor, hand selection may be necessary to achieve optimum noise performance.
Region 3. At high currents, the base current noise dominates.

The load resistor thermal noise and base biasing resistors thermal noise are well below the base resistance thermal noise and do not affect the noise performance of the amplifier, as shall be discussed in Chapter three. An asymptotic plot of the dominant noise components versus collector current is shown below.

Asymptotic Noise Plot vs. Collector Current

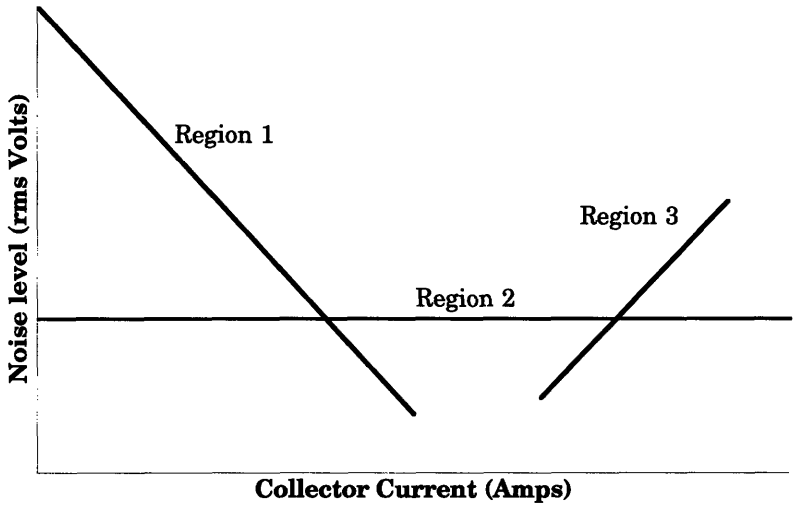

Figure 2-3: Asymptotic plot of noise components vs. collector current

From this analysis, the optimum noise performance of this common emitter amplifier is where the collector current shot noise and the base current shot noise are much less than the base resistance thermal noise. The input noise as calculated by HSPICE follows the MDS curve, thereby confirming the equivalence of the MDS and input noise stated in Chapter one.

Chapter 3

DESIGN PARAMETERS & THEIR EFFECTS ON NOISE PERFORMANCE

3.1 Topology Discussion

There are three basic configurations for a one-stage transistor amplifier: the common base, common collector (emitter follower) and the common emitter. Since this design will have a voltage gain greater than 10, a common emitter amplifier was chosen, as is shown below.

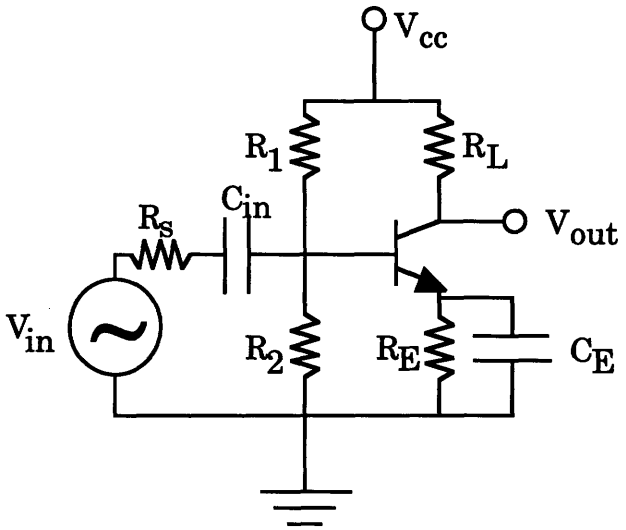

Figure 3-1: Common emitter amplifier topology

3.2 Parameter Variation

The performance of a common emitter amplifier depends on many parameters including the collector to emitter voltage V_{CE}, the quiescent value of the collector current I_C, the load resistor R_L, and the input resistance R_{IN} of the amplifier. Using HSPICE, each of these parameters was varied separately to determine each parameter's effect on the gain, bandwidth, minimum detectable signal, the equivalent input noise and noise figure of the circuit. In Appendix G, a comparison is made between HSPICE and hand calculations of output noise.

Using HSPICE, a common emitter amplifier was designed with the following specifications: Midband voltage gain = 40, 3-dB bandwidth = 100 MHz, and V_{CE} = 1 V. A 3 V power supply was used, with the base biased at 1.6 V, and a quiescent output voltage of 2 V yielding 1 V_{pp} of voltage swing at the output. With this as a reference design, the results of each parameter variation is discussed in the following sections.

3.2.1 I_C Selection

To determine the optimum operating point of the collector current, the collector current was varied from 10 μA to 100 mA. The voltage gain at 100 MHz, 3-dB bandwidth, equivalent input noise and minimum detectable signal are plotted versus collector current.

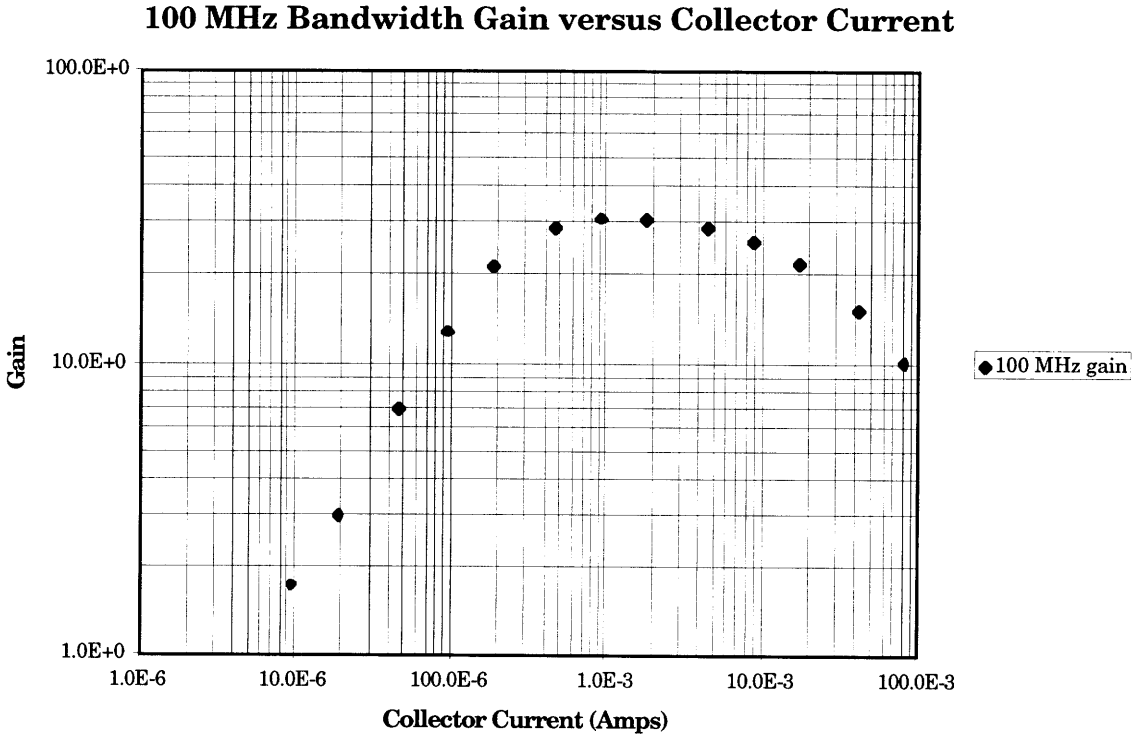

Figure 3-2: 100 MHz bandwidth gain versus collector current

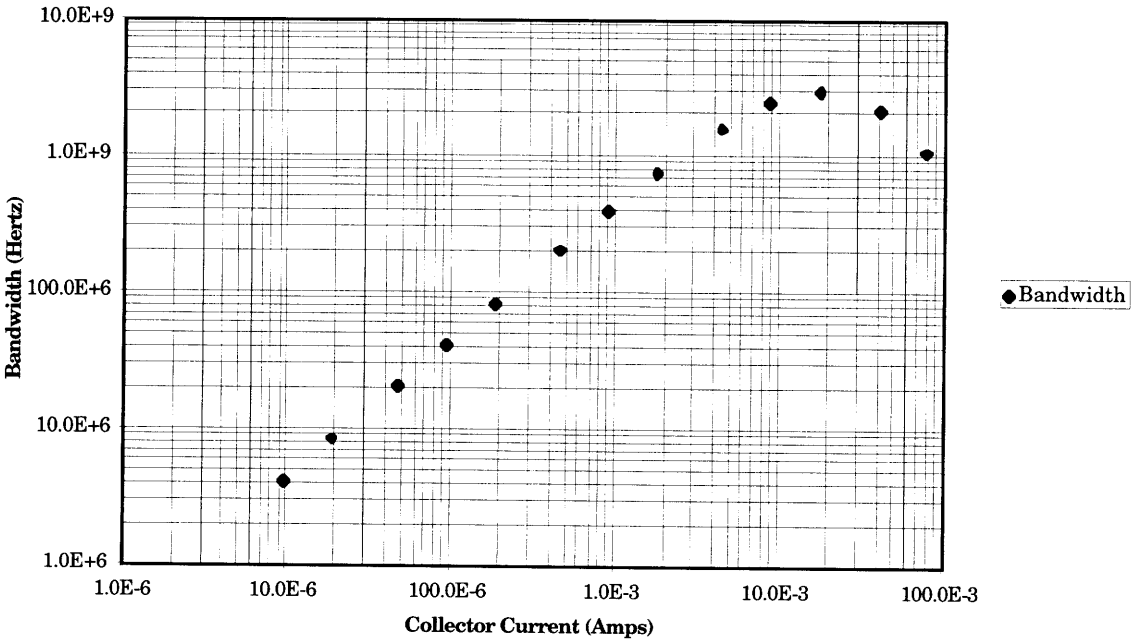

Figure 3-3: 3-dB bandwidth versus collector current

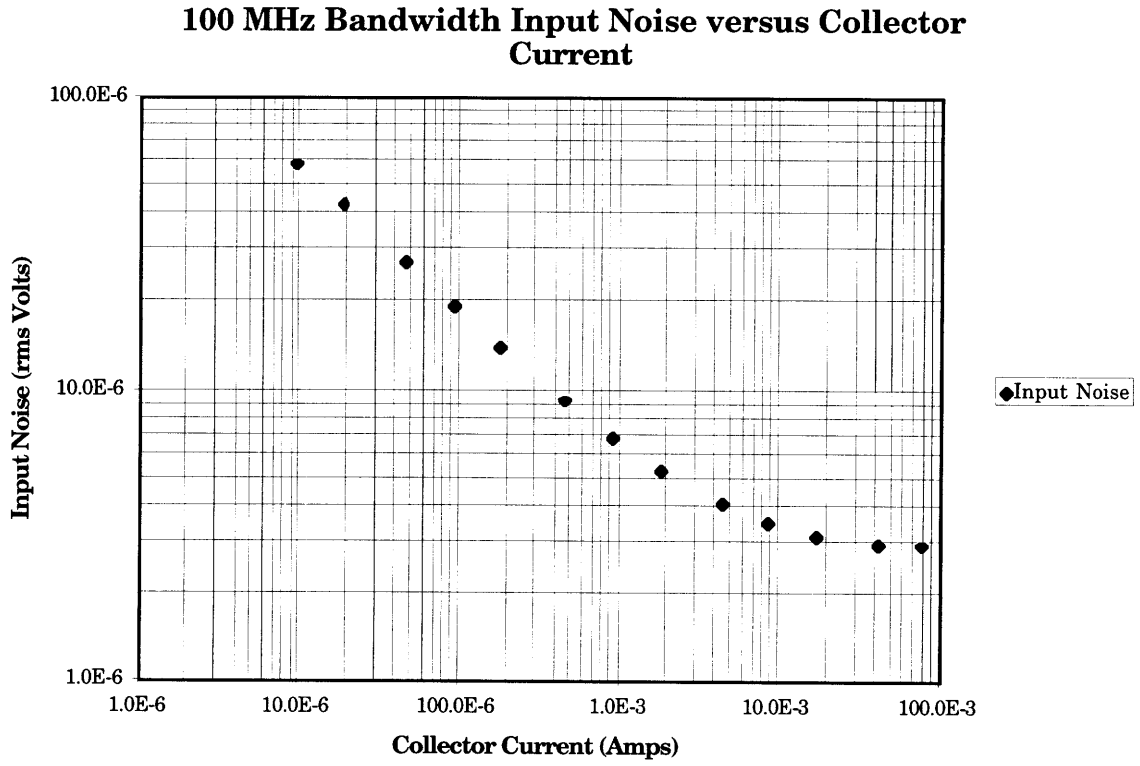

Figure 3-4: 100 MHz bandwidth input noise versus collector current

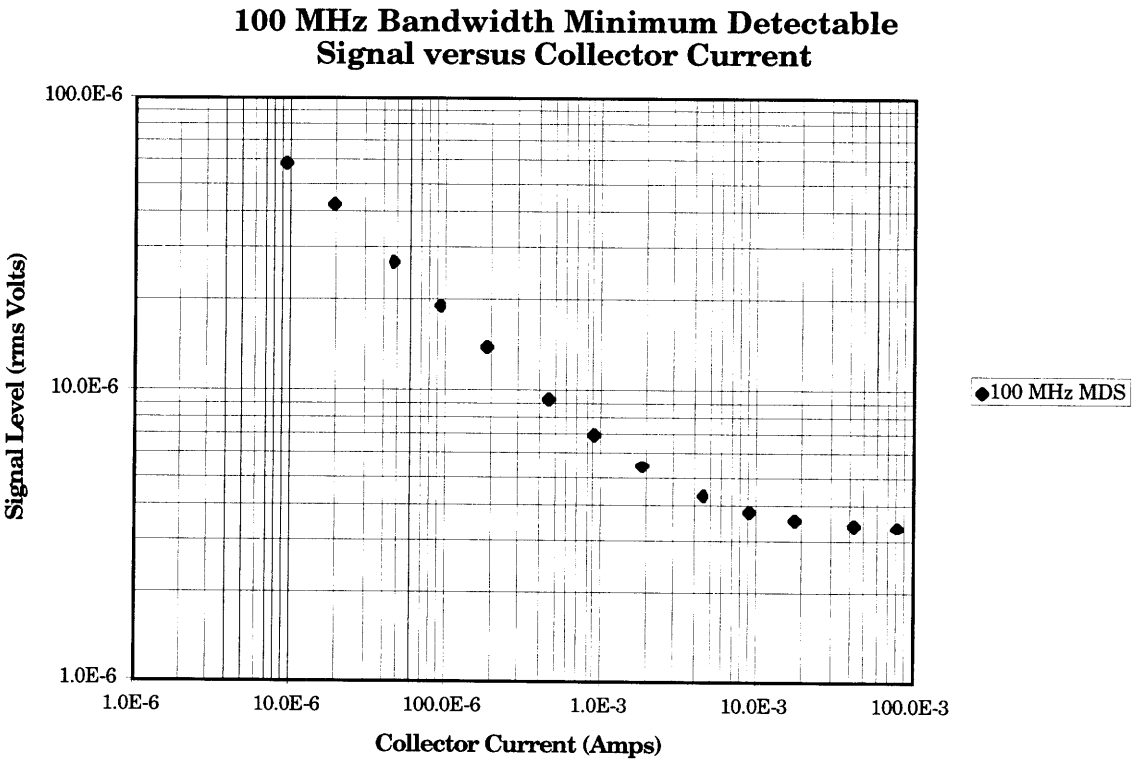

Figure 3-5: MDS versus collector current for 100 MHz bandwidth

The plots indicate that MDS and input noise decrease with increasing collector current and the bandwidth increases with collector current. Since this is a preamplifier, the gain only need be greater than 10, and this is true for collector currents between 100 μA and 100 mA. Therefore, the collector current can be chosen based on the other noise performance characteristics. The effect of I_C on the input noise will be investigated in more detail in Section 3.2.8.

3.2.2 R_L Variations

The midband voltage gain of a common emitter amplifier is, A_V, is $-g_m R_L$. It can be rewritten as $A_v = -\frac{R_L I_C}{25\text{mV}}$ and with the product $I_C R_L$ defined as V_{RL}, the DC voltage drop across the collector resistor. In the following plots, V_{RL} is 1 V, 4 V, 8 V and 16 V corresponding to voltage gains of 40, 160, 320 and 640, respectively.

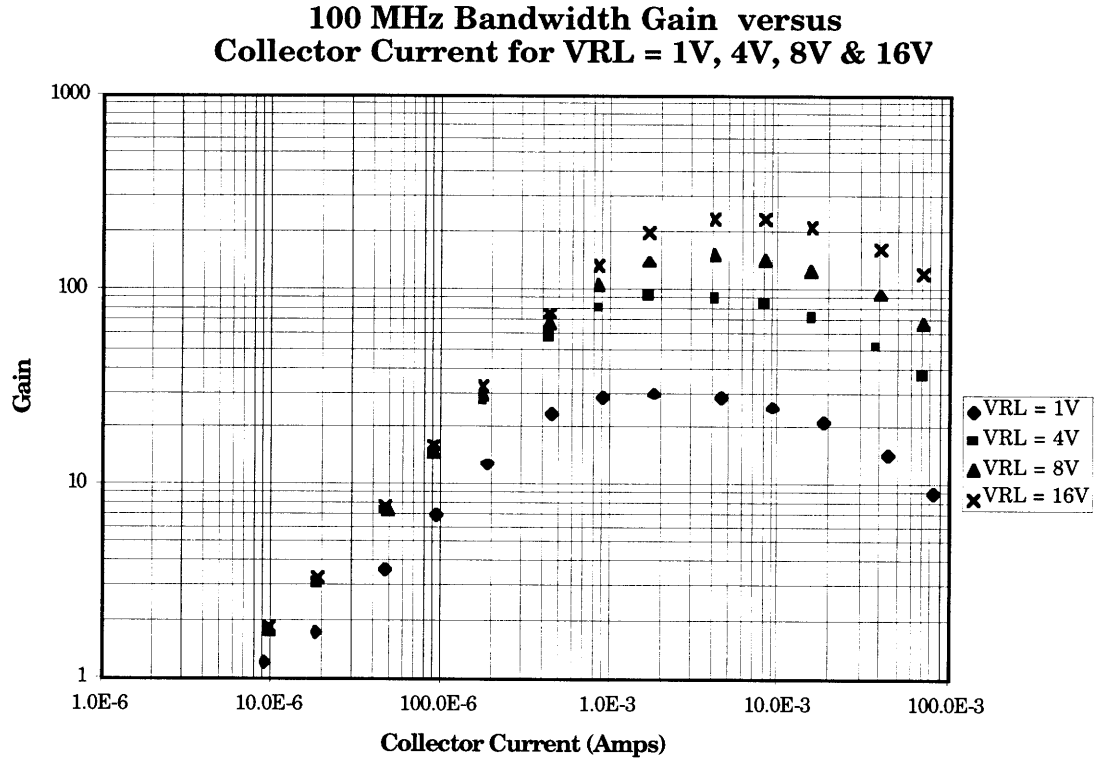

Figure 3-6: Gain versus collector current for V_{RL} =1V, 4 V, 8 V, & 16 V

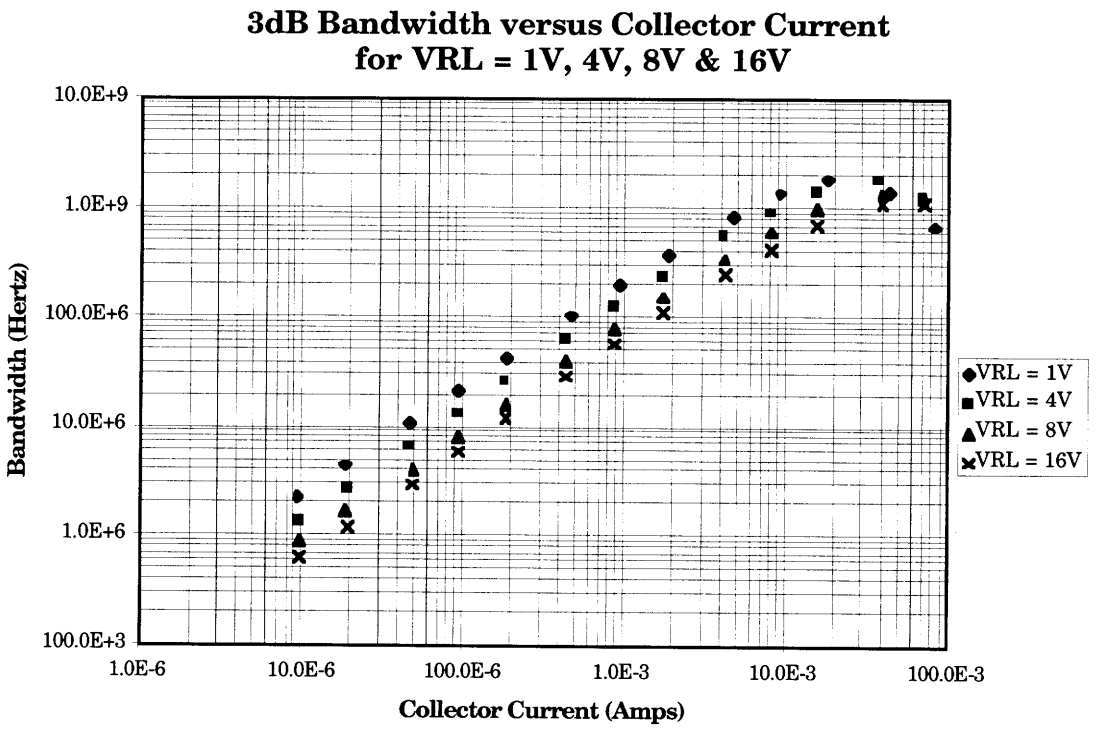

Figure 3-7: 3-dB bandwidth versus collector current for
V_{RL} = 1 V, 4 V, 8 V, & 16 V

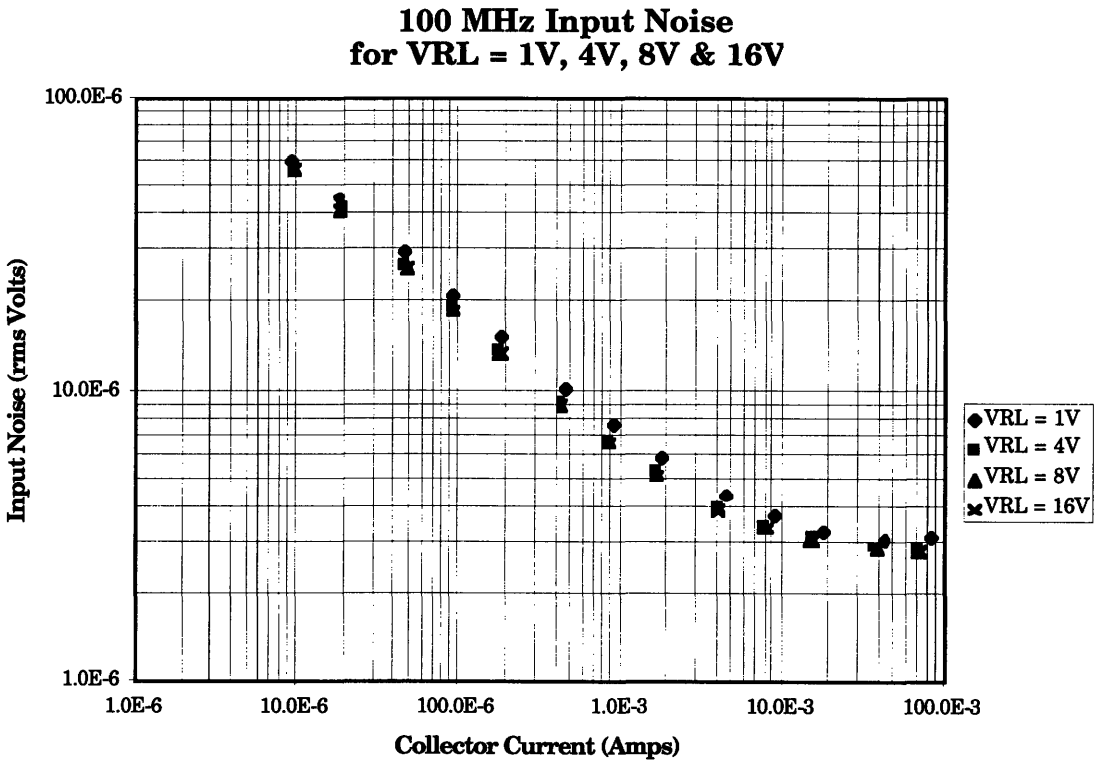

Figure 3-8: 100 MHz input noise versus collector current for V_{RL} = 1 V, 4 V, 8 V, & 16 V

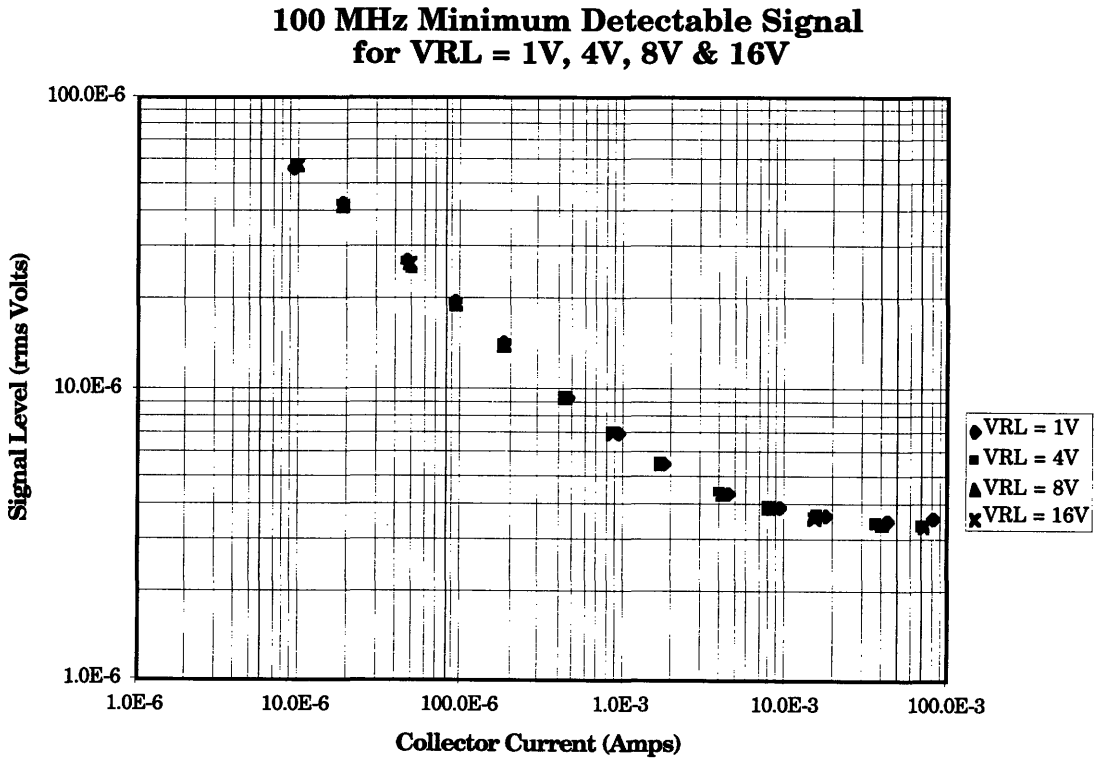

Figure 3-9: 100 MHz MDS versus collector current
for V_{RL} =1 V, 4 V, 8 V, & 16 V

As the plots indicate, V_{RL} has its most significant effect on the gain of the amplifier. Its effects of the MDS and input noise are negligible, while the bandwidth varies inversely with the gain; indicating that there is a finite gain bandwidth product.

3.2.3 V_{CE} Variations

The collector to emitter voltage, V_{CE}, has no first order effect on the small signal properties of the transistor but its second order effects are characterized using HSPICE. Figures 3-10 and 3-11 indicate that the gain and bandwidth increase with increasing collector current. The effects on input noise and MDS are not obvious, so a further study is performed in Section 3.2.7.

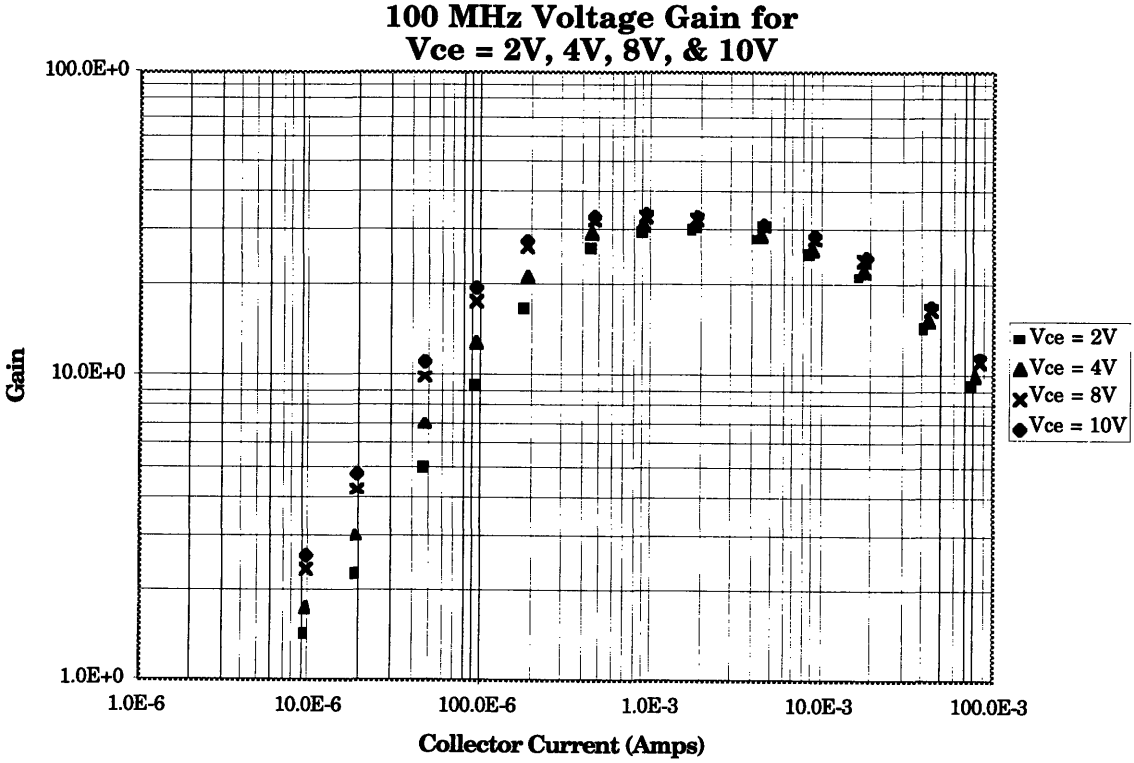

Figure 3-10: 100 MHz gain versus collector current for V_{CE} = 2 V, 4 V, 8 V, 10 V

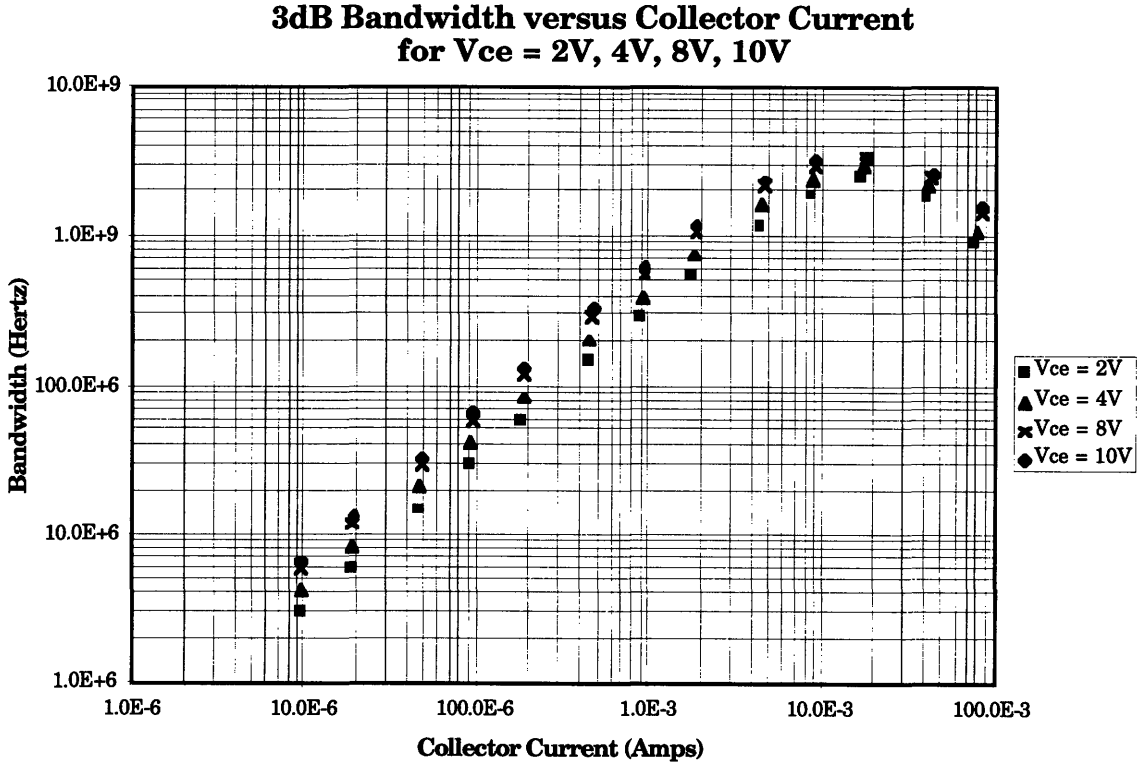

Figure 3-11: 3-dB bandwidth versus collector current for V_{CE} = 2 V, 4 V, 8 V, 10 V

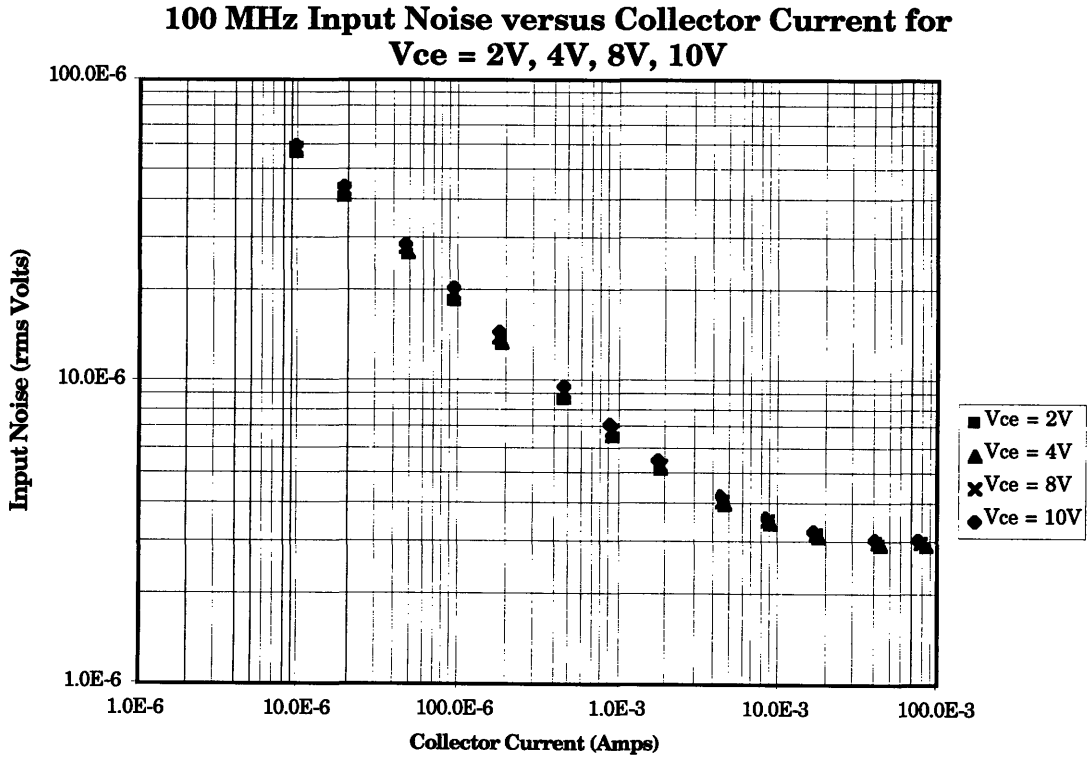

Figure 3-12: 100 MHz input noise versus collector current for V_{CE} = 2 V, 4 V, 8 V, 10 V

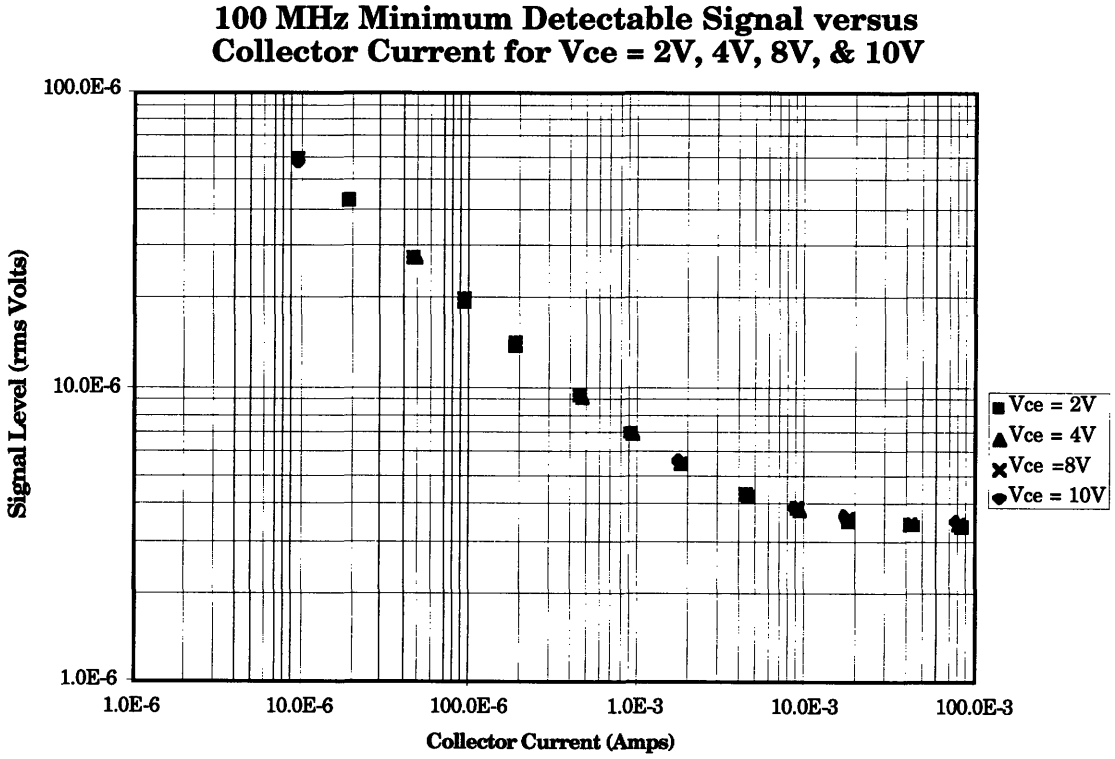

Figure 3-13: 100 MHz MDS versus collector current for V_{CE} = 2 V, 4 V, 8 V, 10 V

3.2.4 R_{IN} Variations

The input resistance to the amplifier depends on the base biasing resistors, R_1 and R_2 and the base to emitter resistance, r_π. However, if the base biasing resistors are chosen to dominate the input resistance expression, $R_1 \| R_2 \| r_\pi$, then the input resistance can be set to 50 ohms that is typical of most function generators and coaxial cable. The input resistance of this amplifier was set to be 50 Ω at different bias currents and the results are plotted below.

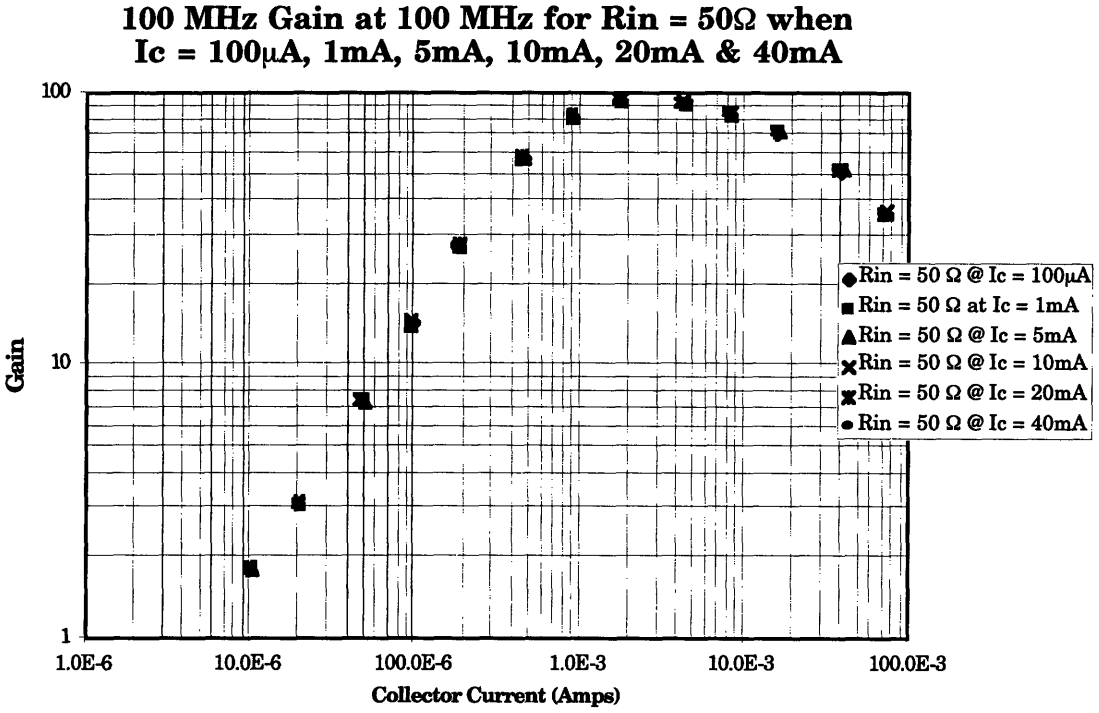

Figure 3-14: 100 MHz gain versus collector current for R_{IN} = 50 Ω when I_C = 100 μA, 1 mA, 5 mA, 10 mA, 20 mA, 40 mA

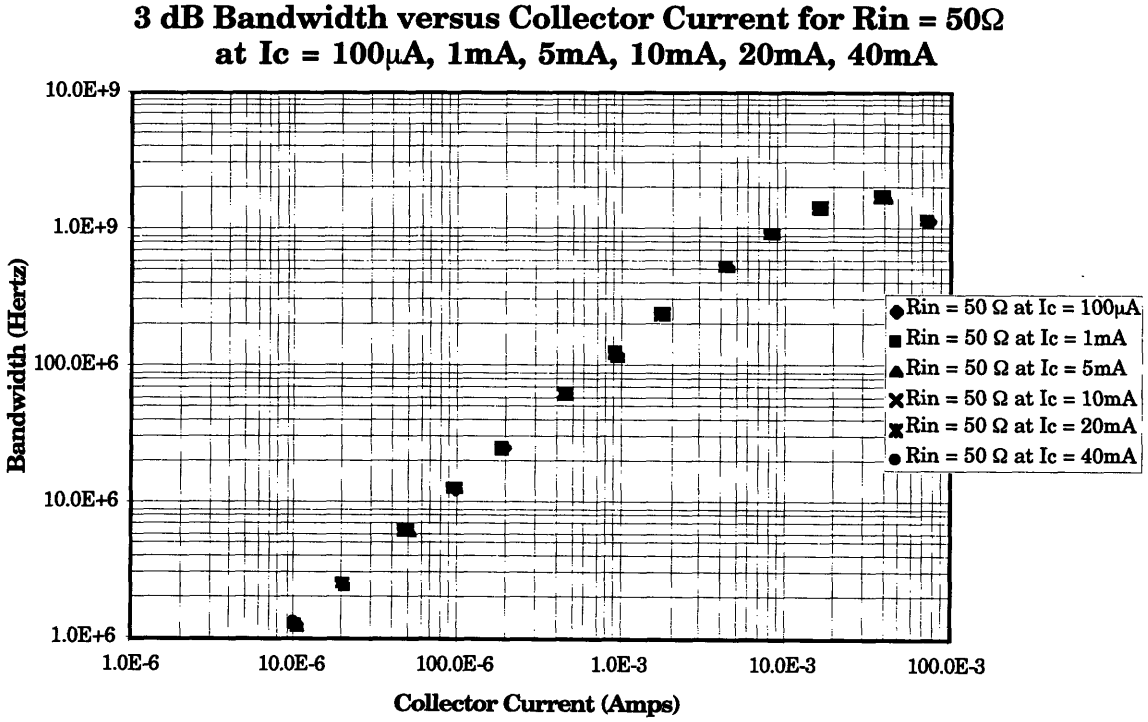

Figure 3-15: 3-dB bandwidth versus collector current for R_{IN} = 50 Ω when I_C = 100 μA, 1 mA, 5 mA, 10 mA, 20 mA, 40 mA

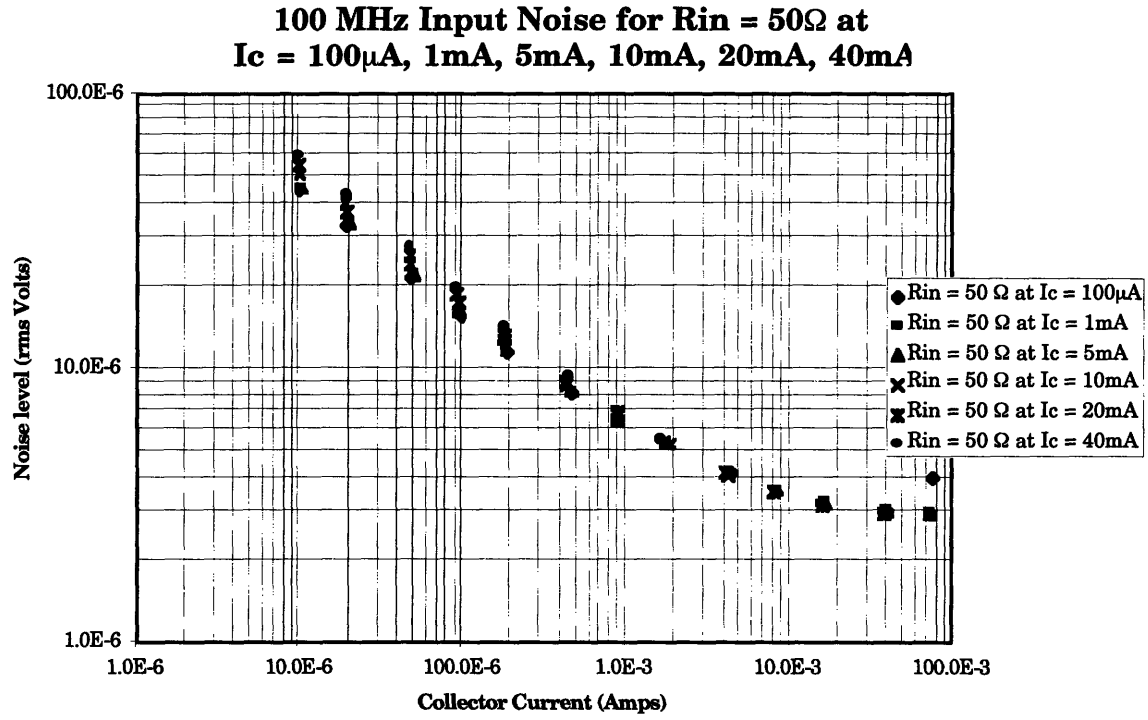

Figure 3-16: 100 MHz input noise versus collector current for R_{IN} = 50 Ω when I_C = 100 μA, 1 mA, 5 mA, 10 mA, 20 mA, 40 mA

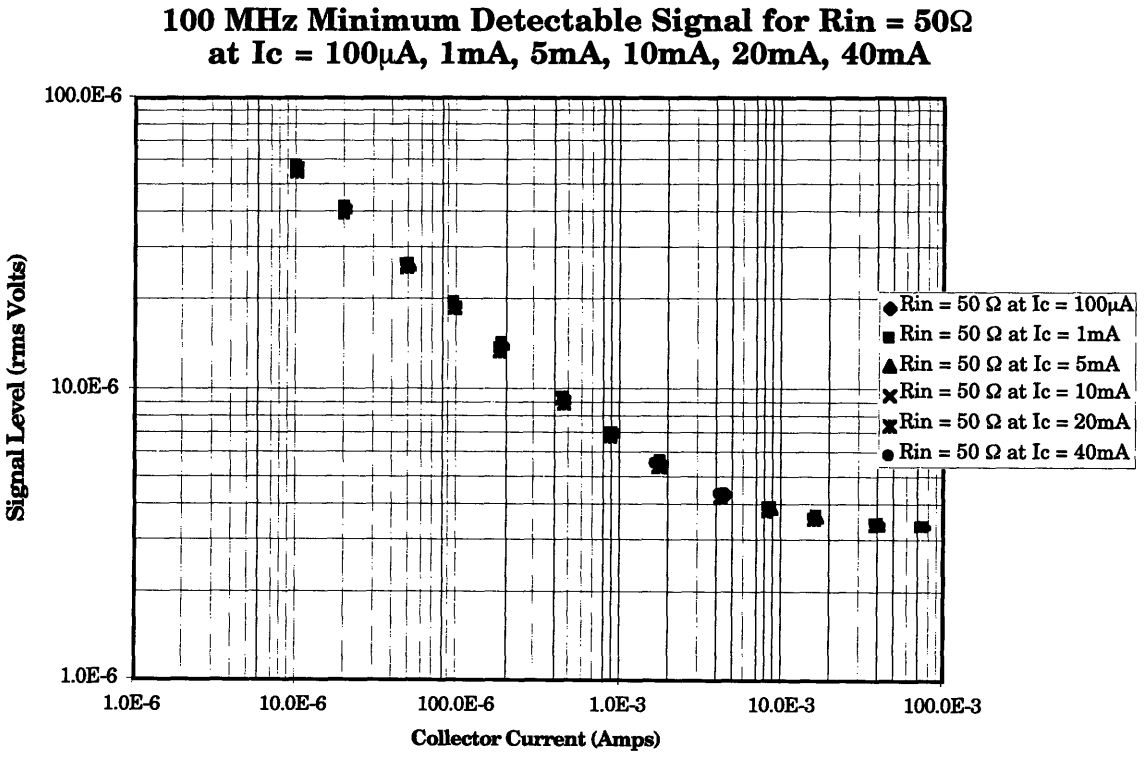

Figure 3-17: 100 MHz MDS versus Collector Current for R_{IN} = 50 Ω when I_C = 100 μA, 1 mA, 5 mA, 10 mA, 20 mA, 40 mA

The input resistance has no effect on the gain of the amplifier, nor does it noticeably affect the bandwidth and MDS of the circuit. The input noise varies by a factor of 1.5 at the high and low extremes of the collector current, however the desired noise performance can be obtained with the proper choice of collector current.

3.2.5 Second Order Effects and Gain Stability

Changes in operating point temperature and transistor β were analyzed also. The design is fairly temperature and β insensitive. These plots are included in the Appendix C.

Also, in Appendix C are the results of a preliminary stability analysis. Reducing the gain of the amplifier by adding emitter degeneration reduced the sensitivity of the voltage gain to collector current. However, the noise performance worsened. Therefore, to maximize the noise performance, no gain stabilization circuitry was added to the amplifier.

3.2.6 Effects of Source Impedance

The source impedance of the circuit coupled to the amplifier can be resistive, capacitive or a combination of the two. Using HSPICE, the source impedance was set to be ideal, $Z_S = 0$, resistive (Z_S = 10, 50, 510 Ω), and capacitive ($Z_S = 1/j\omega 10pF$, $1/j\omega 1000pF$, $1/j\omega 0.1\mu F$). A practical use for low-noise amplifiers is to amplify weak sensor outputs. Since most sensors have impedances that have resistive and reactive components, an example was

simulated with $Z_S = 50 + 1/j\omega 1000pF$. These simulations were performed on amplifiers with a lower 3-dB frequency between one and ten kilohertz and with upper 3-dB bandwidths between 20 and 40 MHz.

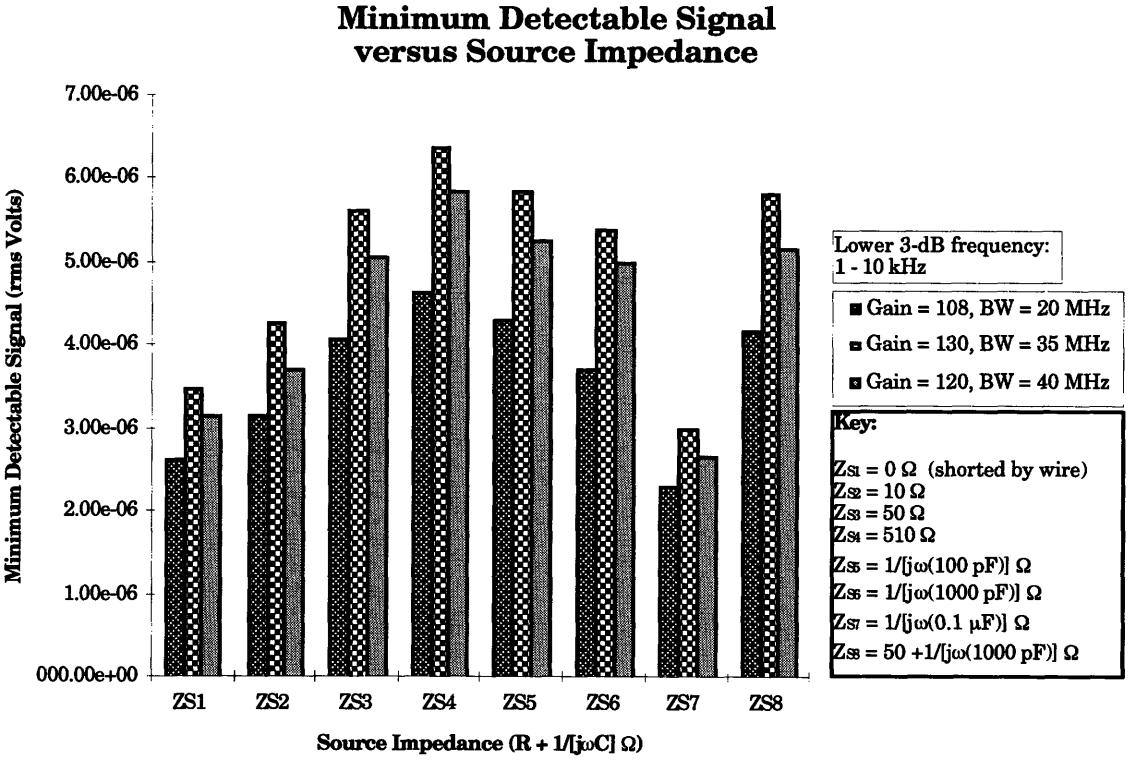

Figure 3-18: MDS versus various source impedances

The Z_{S1} data corresponds to an ideal voltage source ($Z_S = 0$) and will be used as a reference. From the MDS equation stated in Section 2.3, it is evident that the MDS increases with source impedance. For cases Z_{S2}, Z_{S3} and Z_{S4}, the source impedance is 10 Ω, 50 Ω and 510 Ω respectively and from the graph one can see that the MDS is increasing with the source impedance.

For capacitive sources, which in this case are Z_{S5}, Z_{S6} and Z_{S7}, the MDS decreases with increasing source capacitance since the source impedance is inversely related to capacitance. The last case, Z_{S8}, is

representative of a mixed source impedance. Again, the source is non-ideal, so, as expected, its MDS is higher than that of the ideal source.

3.2.7 Constant I_C with V_{CE} variations

In Section 3.2.3, a preliminary study of the effects of V_{CE} were inconclusive pertaining to the noise performance of the amplifier because too many parameters were being varied simultaneously. In this section, all parameters are held constant except V_{CE}.

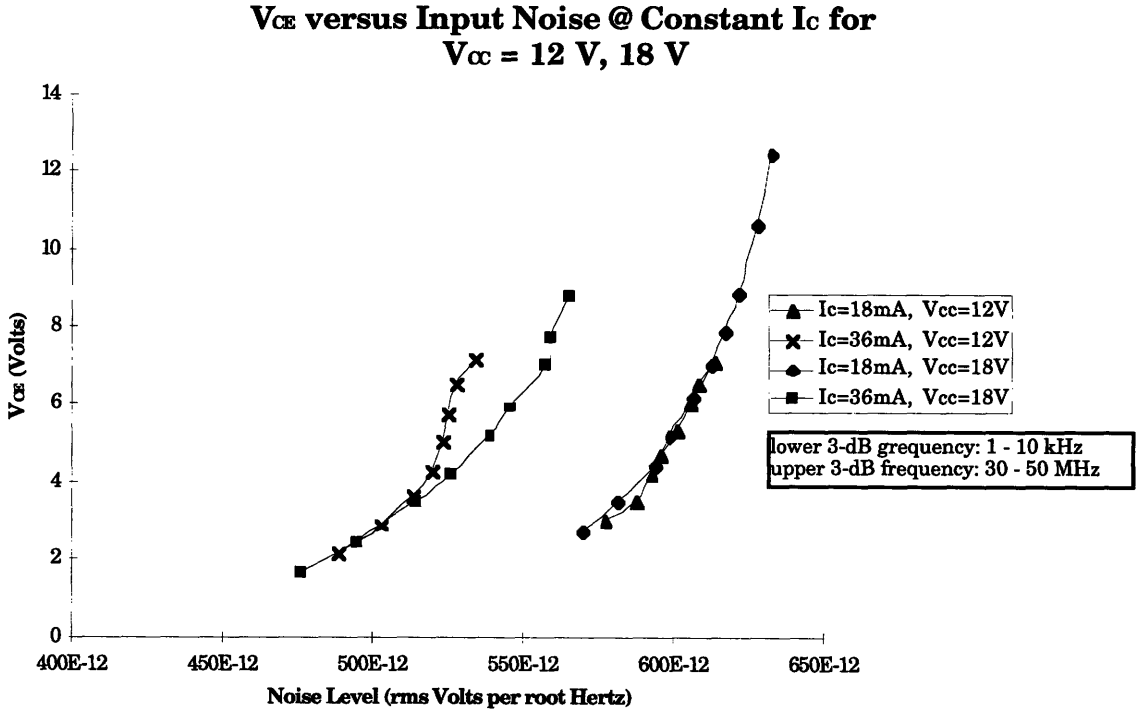

Figure 3-19: V_{CE} vs. Input Noise at I_C=18, 36 mA

From the above graph, it is evident that the input noise decreases with decreasing V_{CE}. Also, one can see that the higher collector current is preferable, which agrees with figure 3-4.

3.2.8 Effects of I_C on Input Noise

As stated in Section 3.2.1, the input noise decreases with increasing collector current. This effect is more pronounced in the following graph, where the collector current was varied while V_{CE} was fixed.

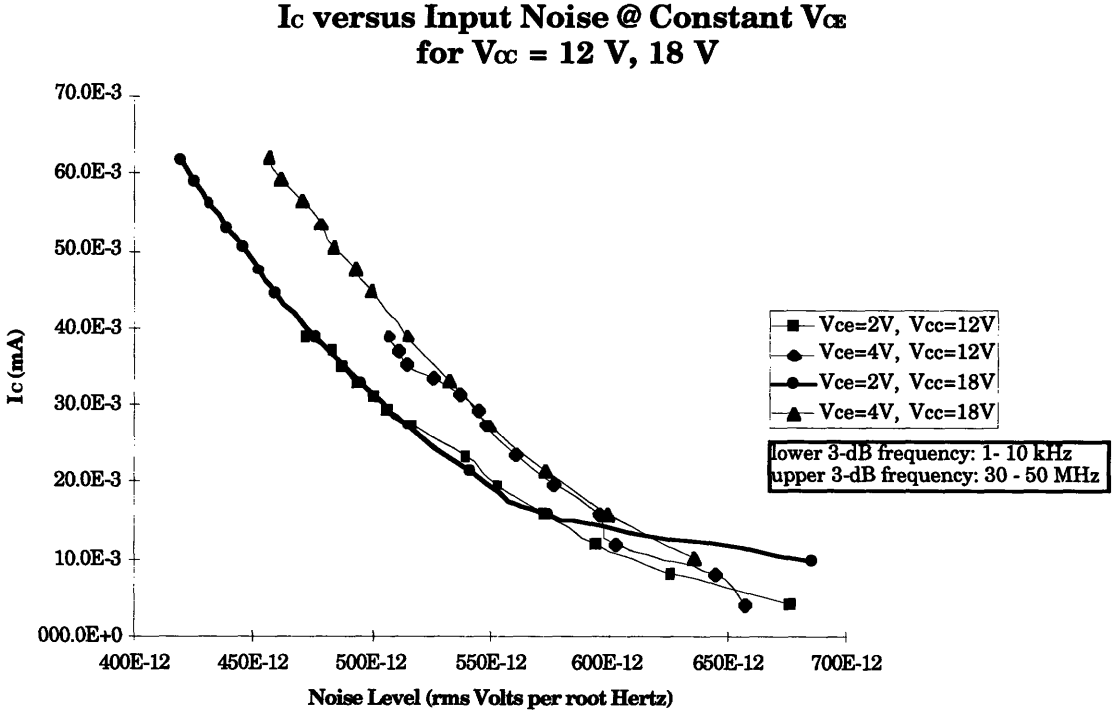

Figure 3-20: I_C vs. Input Noise at V_{CE} = 2 V, 4 V

3.3 Effects of Parameter Variation on Noise Figure

From the previous sections, the collector current had the most pronounced effect on the performance of the amplifier. Also, the collector-to-emitter voltage had a direct effect on the bandwidth of the amplifier. In this section, the effects of these parameters on the noise figure of the amplifier will be investigated.

3.3.1 Constant I_C with V_{CE} Variations

Using HSPICE, the collector current was kept constant at 18 mA and 36 mA, allowing V_{CE} to vary. This variation was done at two different supply voltages: 12 V and 18 V. The noise figure was calculated based on the total output noise voltage computed by HSPICE. The formula used was:

$$20\log_{10}\frac{\text{total output noise}}{\text{gain} * 50 \text{ ohm noise voltage}}.$$

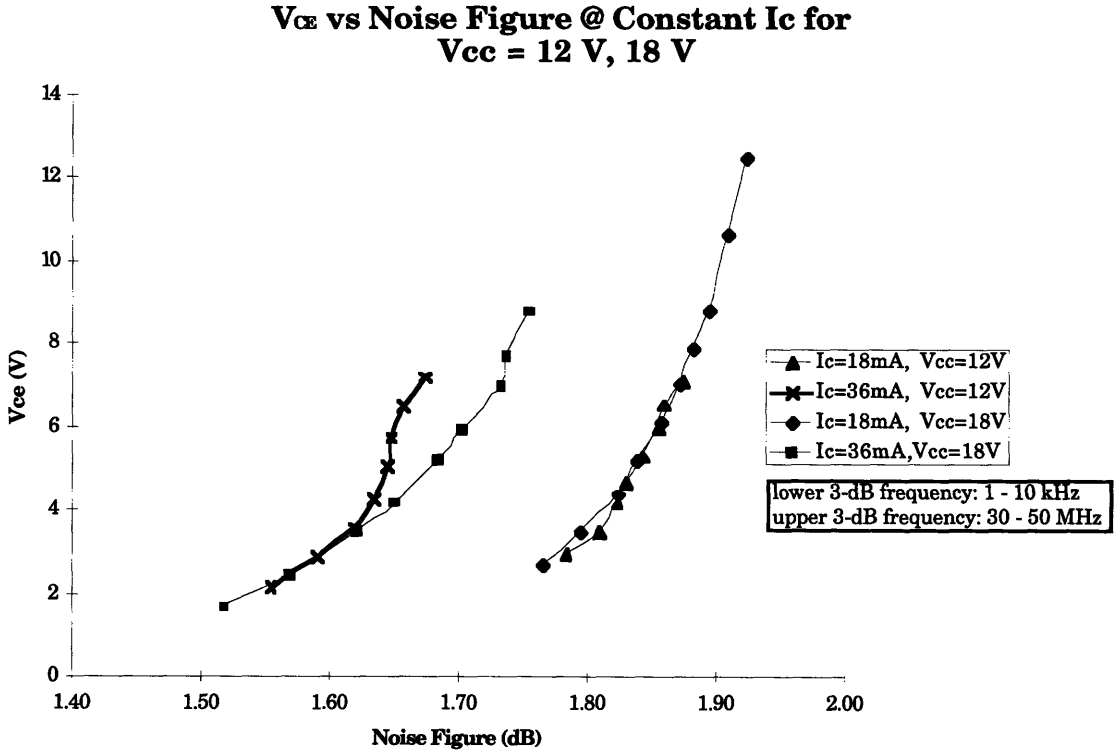

Figure 3-21: V_{CE} versus noise figure for constant collector current

From this graph it is evident that the noise figure decreases with decreasing V_{CE}. The supply voltage V_{CC} causes negligible variations in the noise figure. Therefore, in the final design, V_{CC} can be chosen with respect to what power supplies are available.

3.3.2 Constant V_{CE} with I_C Variations

The collector to emitter voltage V_{CE}, was held constant while varying the collector current. As in the previous section, this was performed at two collector supply voltages: 18 V, and 12 V.

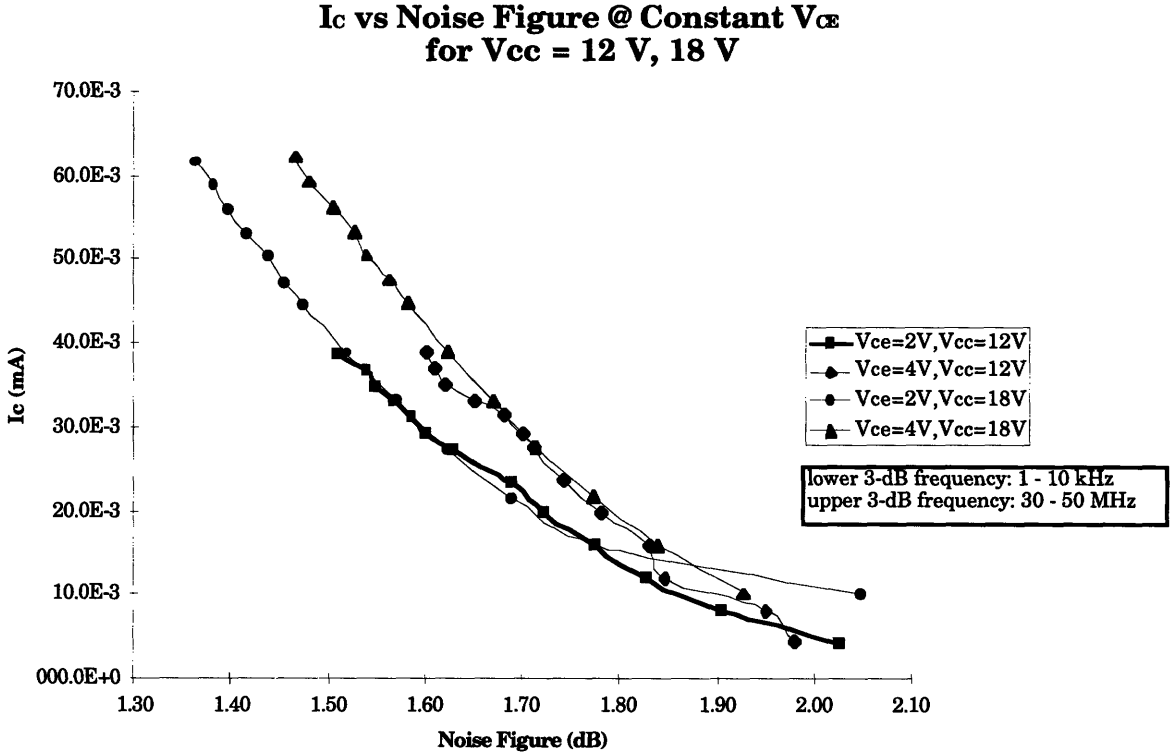

Figure 3-22: Collector current versus noise figure for constant V_{CE}

This graph shows that the noise figure varies inversely with the collector current. The supply voltage V_{CC}, has no direct effect on the noise figure.

3.3.3 Noise Figure Dependence on Input Resistance

The parameter of interest now is the input resistance of the amplifier. The previous V_{CE} and I_C variations were generated by simulating amplifiers with 50 Ω input impedances. Now, the input resistance was set to 100 Ω and compared to a corresponding 50 Ω system.

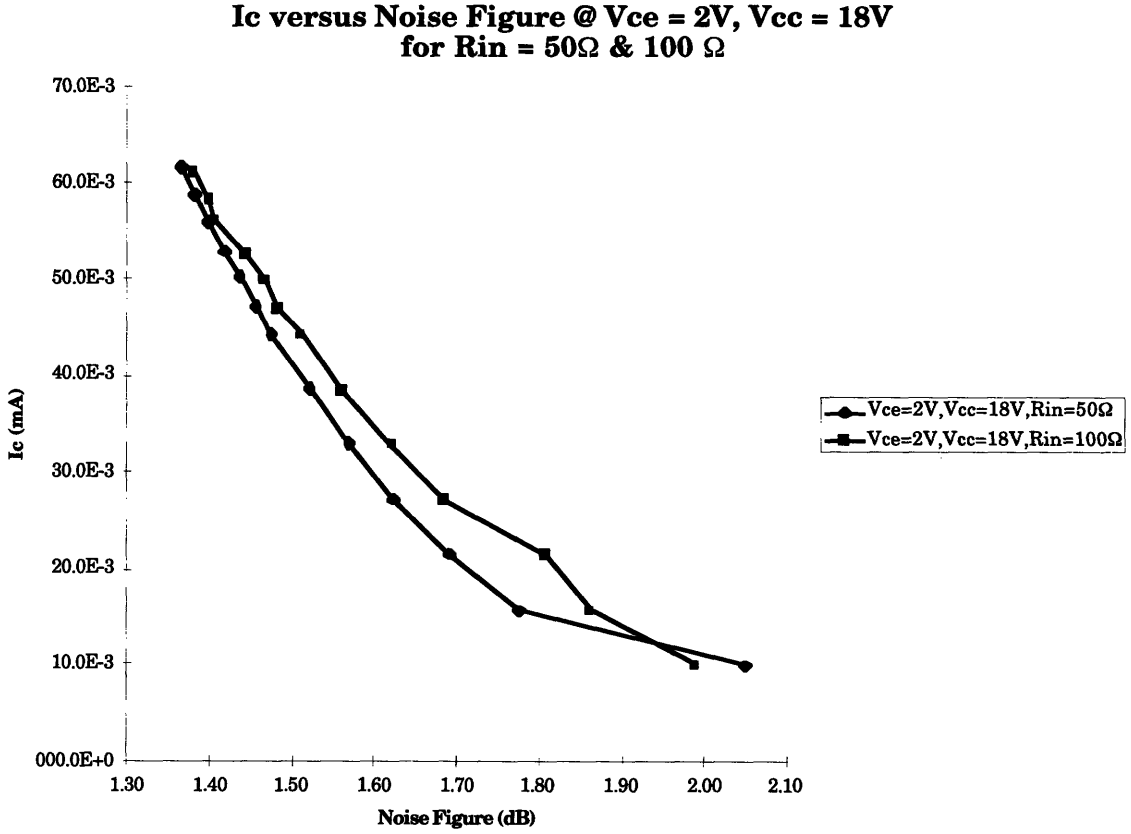

Figure 3-23: Collector current versus noise figure for R_{IN} = 50 Ω, 100 Ω

According to the above graph, the input resistance of the amplifier has a negligible effect on the noise figure. At this point, all parameters that affect the noise performance of the amplifier have been identified. In the next chapter, the HSPICE predictions and trends presented in this chapter will be compared to actual lab results.

Chapter 4
LABORATORY TESTING

In this chapter, specific amplifiers will be designed and analyzed in detail. Three circuits, with upper bandwidths of 6 MHz, 50 MHz, and 200 MHz; and lower bandwidths, as calculated in Appendix C.3, between 1 - 10 kHz will be presented. The succession of designs allows for the development of a correlation between lab and theory and it allows for a correction of the model, as it becomes more complex due to more pronounced parasitic effects as higher bandwidths are achieved.

4.1 The 5-10 MHz Amplifier

The first amplifier was designed to have a bandwidth between five and ten megahertz. The gain was loosely specified as at least 10. The open circuit time constants, HSPICE, MATLAB and laboratory results are presented in the following sections. The topology with all parameter values is:

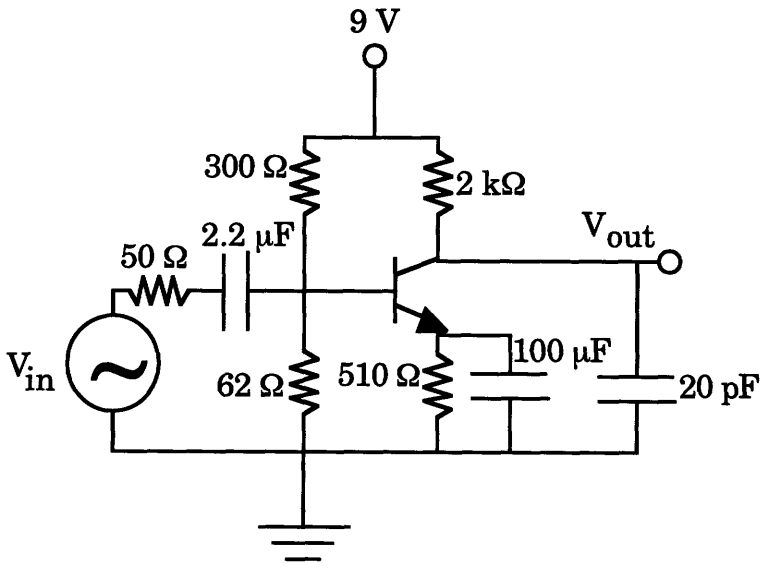

Figure 4-1a: The 5-10 MHz amplifier topology

The layout of the actual circuit used is shown in Figure 4-1b.

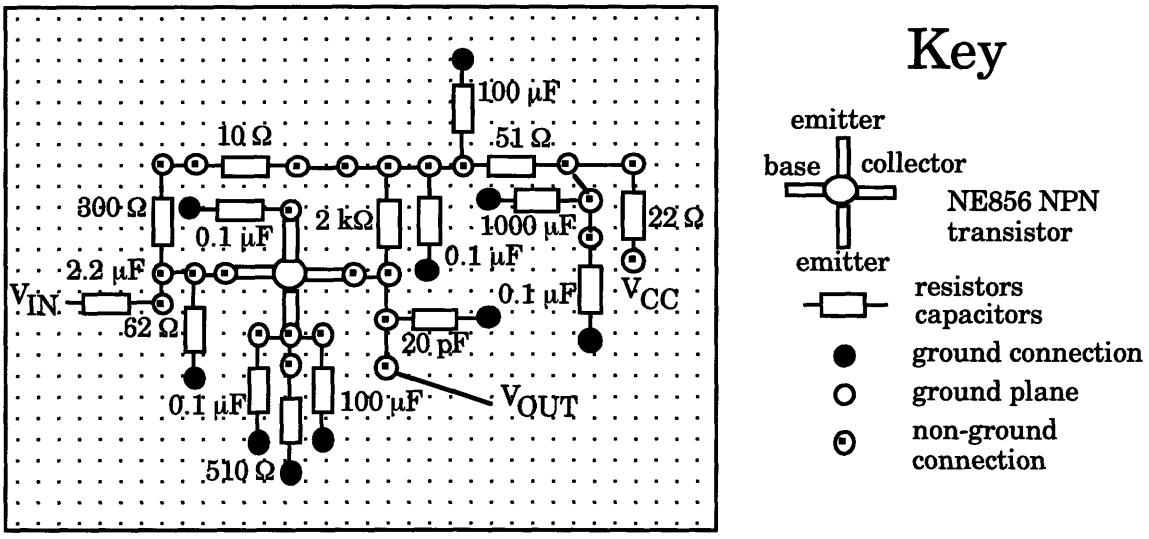

Figure 4-1b: Layout of the circuit implementation of the 5-10 MHz amplifier

4.1.1 Open Circuit Time Constant Analysis

A full derivation of bandwidth via the open circuit time constants for a common emitter amplifier is given in the Appendix. The results for V_{CC} = 9V, and I_C = 1.6 mA are:

$$\tau_{\pi o} = 2.2\text{x}10^{-10}\text{s}$$

$$\tau_{\mu o} = 9.46\text{x}10^{-10}\text{s}$$

Assuming, all other parasitic capacitances are negligible, the bandwidth of this amplifier is 136 MHz. To decrease the bandwidth of the amplifier, a dominant time constant of 31.3 ns was added. This was achieved by the addition of a 20 pF capacitance at the output. With this additional capacitance, this analysis predicted the desired lower f_{3db} point of 4.9 MHz.

4.1.2 HSPICE and MATLAB Predictions

This circuit's performance was predicted by HSPICE and for MDS, MATLAB. The results are summarized in the table below:

Ic	Gain	Bandwidth	Input Noise	MDS	Noise Figure	Rin
1.6 mA	99	6.5 MHz	2.8 μV	2.4 μV	2.26 dB	50 Ω

Table 4-1: HSPICE & MATLAB predictions for the 5-10 MHz amplifier

4.1.3 Lab Results

The 6 MHz amplifier was built and its performance was measured as shown in Appendix H. The results are:

Ic	Gain	Bandwidth	Input Noise	Noise Figure	Rin
1.75 mA	100	6.3 MHz	2.9 μV	2.73 dB	50 Ω

Table 4-2: Lab results for the 5-10 MHz amplifier

The lab results are very similar to the HSPICE and MATLAB predictions. The discrepancy in noise figure indicates that the transistor selected does not have the same parameters as the HSPICE model. There was no direct way to measure the MDS in the lab.

4.2 The 30-50 MHz Amplifier

The next amplifier that was built was to have a bandwidth in the 30 - 50 MHz range. Due to the higher bandwidth of this amplifier, the noise measurements required more precaution. A low noise emitter-follower stage was added to the original common emitter amplifier yielding the following topology:

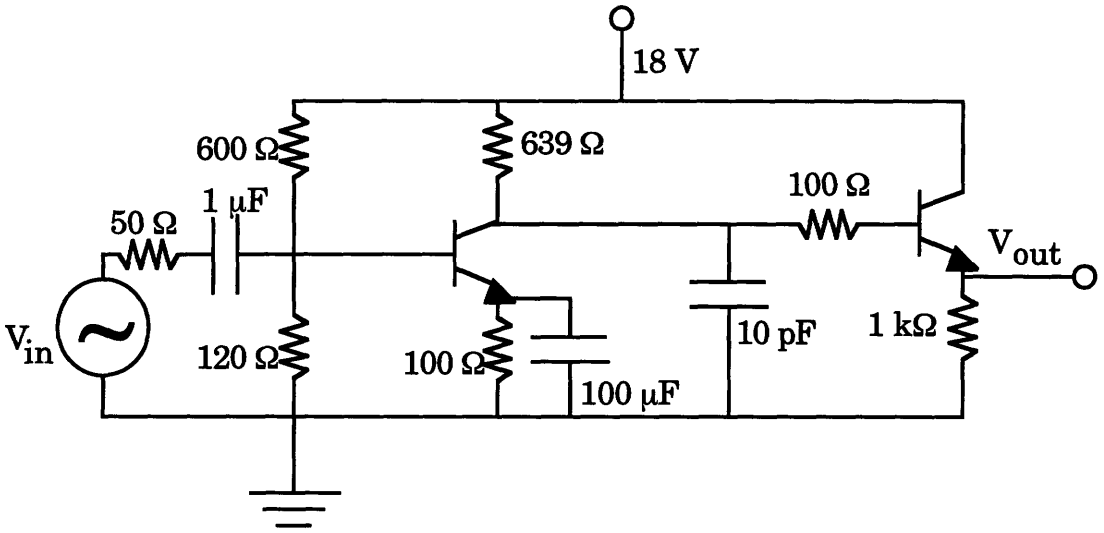

Figure 4-2a: The 30-50 MHz amplifier topology

The layout of the actual 30 - 50 MHz bandwidth amplifier is show in below.

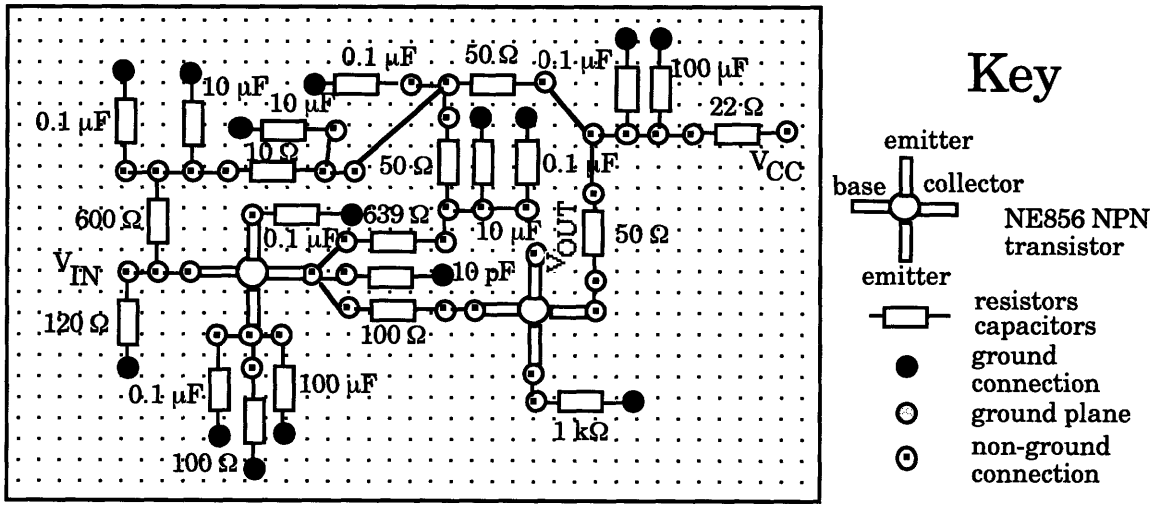

Figure 4-2b: Layout of the circuit implementation of the 30 - 50 MHz amplifier

4.2.1 Open Circuit Time Constants

The target bandwidth for this amplifier was between 30 and 50 MHz. Since the load resistor needs to be large to have a significant gain, the output resistance of the amplifier needed to be lowered to be able to drive a 50 Ω

measurement load. To achieve this, an emitter follower stage was added to the circuit. The open circuit time constants for this two-stage circuit are:

$$\tau_{\pi o1} = 3.17x10^{-10}s$$
$$\tau_{\mu o1} = 6.55x10^{-10}s$$
$$\tau_{\pi o2} = 2.49x10^{-11}s$$
$$\tau_{\mu o2} = 4.25x10^{-11}s$$

This predicts a bandwidth of 146 MHz. To reduce the bandwidth, a dominant time constant of 4.6 ns was created by placing a 10 pF capacitor at the collector of the common emitter amplifier, which caused a overall time constant of 5.6 ns. This changed the predicted bandwidth to 28 MHz.

4.2.2. HSPICE and MATLAB Predictions

MATLAB and HSPICE predict this circuit to operate with the following characteristics:

Ic	Gain	Bandwidth	Input Noise	Noise Figure	Rin
21.5 mA	115	46.7 MHz	4 μV	1.81 dB	50 Ω

Table 4-3: Performance predictions for the 50 MHz amplifier.

4.2.3 Lab Results for the 30-50 MHz Bandwidth Amplifier

Ic	Gain	Bandwidth	Input Noise	Noise Figure	Rin
23.5 mA	129	30 MHz	5.1 μV	2.36 dB	50 Ω

Table 4-4: Performance of the 30-50 MHz amplifier in the lab.

The noise figure was 30% higher than predicted. This discrepancy indicates that device selection may be necessary to attain optimum performance, there may be errors in the HSPICE model, or ambient noise may be contributing to the noise measurement.

4.3 The 100-200 MHz Design

The design of an amplifier with 100 MHz to 200 MHz of bandwidth is presented in this section. Since the bandwidth is high, more attention has to be paid to rejecting outside disturbances. This crosses the boundaries of this project therefore only the design was done with no laboratory testing. The circuit with all of its component values is shown in Figure 4-3.

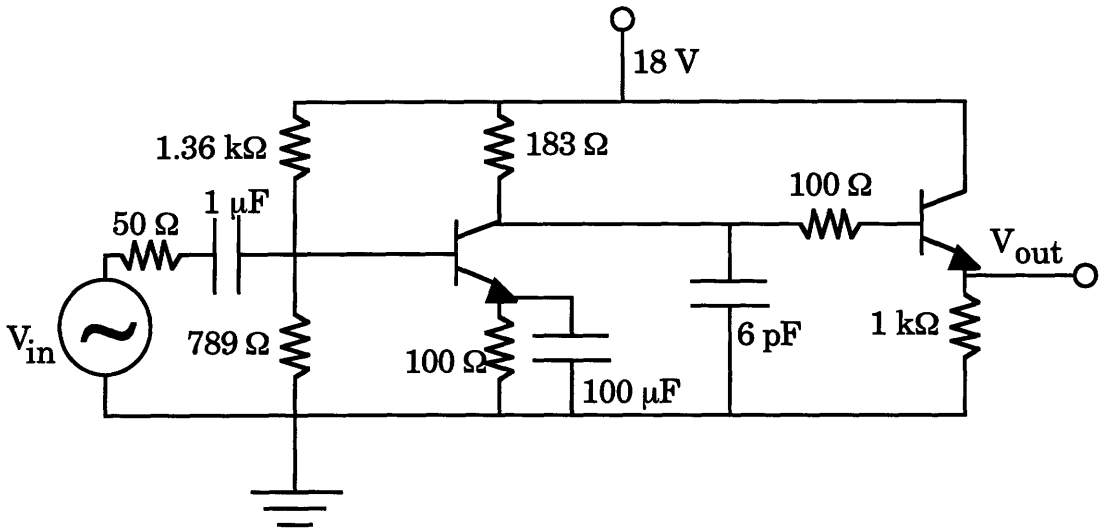

Figure 4-3: The 200 MHz amplifier topology

4.3.1 Open Circuit Time Constants

In order to achieve this high bandwidth, the emitter follower stage is crucial. The open circuit time constants for this amplifier are:

$$\tau_{\pi o1} = 1.1 \text{ ns}, \quad \tau_{\mu o1} = 1.7 \text{ ns}$$

$$\tau_{\pi o2} = 25 \text{ ps}, \quad \tau_{\mu o2} = 11.2 \text{ ps}$$

$$\tau_{ol} = 0.7 \text{ ns}$$

4.3.2 HSPICE and MATLAB predictions

The performance predictions of the 200 MHz amplifier are summarized in Table 4-5.

Ic	Gain	Bandwidth	Input Noise	Noise Figure	Rin
36 mA	75	173.3 MHz	6.4 μV	1.56 dB	50 Ω

Table 4-5: Performance predictions for the 100-200 MHz amplifier.

4.4 Laboratory Confirmation

Observations in the lab confirmed the HSPICE and MATLAB trends for noise figure stated previously. With the collector to emitter voltage increasing and the collector current constant, the noise figure will increase. Also, at a fixed collector to emitter voltage, the noise figure increases with increasing collector current. The data is summarized as follows:

Constant Ic				
Ic (mA)	**VCE (Volts)**	**Gain**	**BW (Hertz)**	**NF (dB)**
23.5E-3	3	115.5	30.0E+6	2.36
23.5E-3	5	101	33.0E+6	2.54
23.5E-3	10	53.76	43.8E+6	2.74
Constant VCE				
Ic (mA)	**VCE (Volts)**	**Gain**	**BW (Hertz)**	**NF (dB)**
23.5E-3	5	101	33.0E+6	2.54
16.5E-3	5	120	23.3E+6	2.62
12.5E-3	5	118	15.0E+6	2.96

Table 4-6: Noise figure for I_C and V_{CE} variations

Displaying this data graphically makes the trends easier to recognize and allows for correlation to figures 3-19 and 3-20.

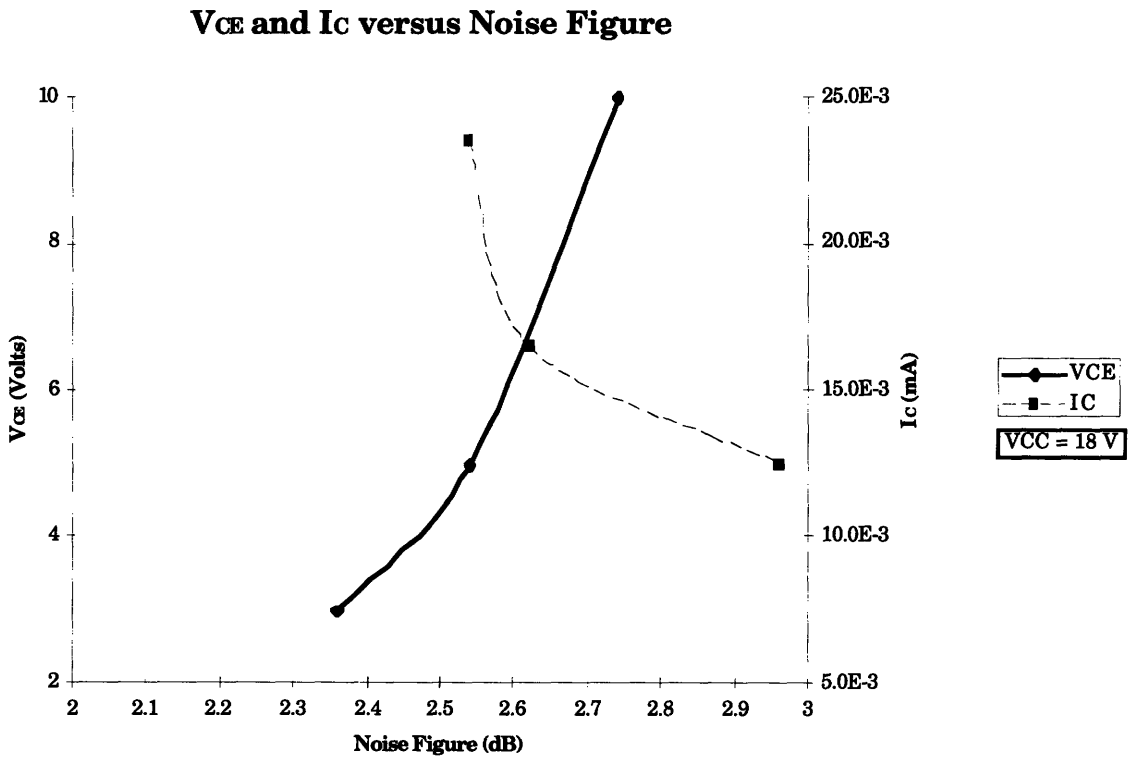

Figure 4-4: Measured V_{CE} and I_C versus noise figure for the 30-50 MHz amplifier

4.5 Discrepancy Analysis

The amplifiers were noisier than predicted by HSPICE & MATLAB. The discrepancies may be due to a combination of the following sources: outside interference, errors in measurement, and errors in the HSPICE/MATLAB models. The HSPICE parameter values for the NE856 low noise bipolar transistor were obtained from the manufacturer and were used in both HSPICE and MATLAB simulations. The transistors used in the lab may not have the parameters used in the model. It may be noisier than the transistor used in the model, so hand selection will be necessary to find the best transistor in a batch. Also, since metal film resistors were not available, the carbon film resistors that were used may exhibit more than just thermal noise.

The amplifiers' performance were measured as shown in block diagrams of Appendix H. There may be more accurate configurations or better instrumentation for making these sensitive noise measurements. Nevertheless, the changes in noise with component and/or operating point changes were shown to be consistent with theory. Low-noise trade-offs were, therefore, established.

A comparison of the laboratory measurements with HSPICE calculations is shown in Figure 4-5. The laboratory measurement curves have approximately the same slope as the HSPICE calculated curves, suggesting that the discrepancy can be expressed as a linearly, e.g. m*NF + b. The slope of the discrepancy, m, is the difference between the slopes of the HSPICE calculated curve and the curve of the laboratory measured data points. The graph suggests that m should be small, however this was not confirmed since there are not enough data points. The offset, b, is roughly 0.6 dB. Again, this is an estimate that should be confirmed with more measurements.

To shield a circuit from ambient noise, it should be installed in a Faraday cage. In this case, the cage was made of aluminum sheet metal rather than a thicker aluminum or copper, which is a better conductor. Although better shielding may have been possible, the tests still showed the basic noise response characteristics.

Another possible factor is that the base biasing resistors generated more noise than expected from theoretical analysis. Carbon film resistors were used instead of metal film resistors, which have better noise performance.

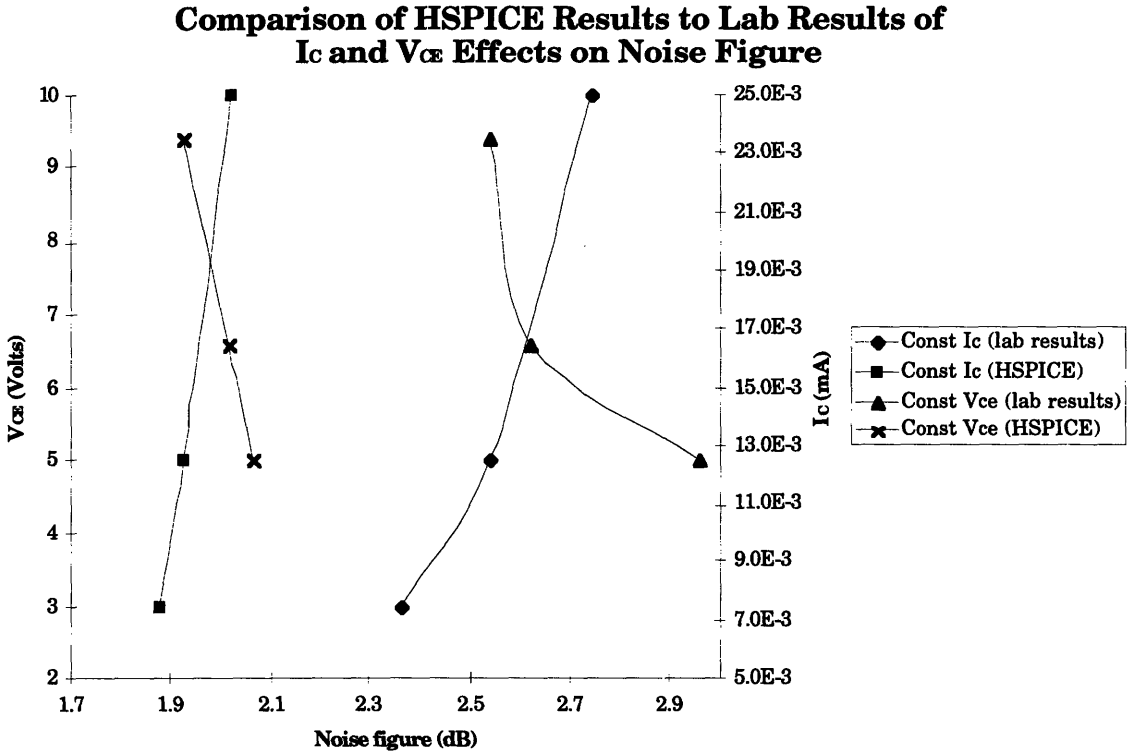

Figure 4-5: Comparison between HSPICE and laboratory results of I_C and V_{CE} effects on Noise Figure

4.6 Other Designs

The amplifiers presented thus far in this chapter have been optimized for 50 Ω systems. However, if there was no cable impedance constraint placed on the design of the amplifier, the noise performance can be improved further. Minor changes were made to the 50 MHz and 200 MHz designs to yield the following predictions.

Ic	Gain	Bandwidth	Input Noise	Noise Figure	Rin
36 mA	106	42.6 MHz	3.4 μV	1.64 dB	25 Ω
36 mA	110	140.3 MHz	4.9 μV	1.4 dB	25 Ω

Table 4-7: Enhanced performance predictions for the 30-50 MHz & 100-200 MHz amplifiers.

Chapter 5

CONCLUSIONS AND RECOMMENDATIONS

The goal of this project was to examine the effects of design parameters on the noise performance of a bipolar transistor amplifier. The noise performance can be quantified by two factors: noise figure (NF) and minimum detectable signal (MDS). The noise figure approach, is an older more common unit of measure but it does not lend itself to predicting the noise generators as does the MDS.

There are three noise generators in a transistor, exhibiting two types of noise: thermal and shot noise. Shot noise is present in the base and collector currents. Thermal noise is only present in the base resistance, r_b, since it is the only physical resistance in the hybrid-pi model. The other resistances in the hybrid-pi model, r_π and r_o, don't contribute thermal noise, since they are modeling resistors.

The minimum detectable signal along with its shot and thermal noise components are plotted in Figure 2-2. At low currents, the MDS is dominated by collector current shot noise. The minimum value of the MDS is set by the r_b thermal noise until at high currents when the base current shot noise becomes the most significant noise component.

The two main parameters that influence the noise performance of an amplifier are collector current and collector to emitter voltage. Noise figure and input noise decrease as collector current increases, as indicated by Figures 3-20 and 3-22. Figure 3-21 shows that the noise figure increases with increasing collector to emitter voltage, as does figure 3-19 indicate the same dependence on the input noise. These two pairs of graphs suggest that there is a one-to-one correspondence between the noise figure, and the input noise, which is equal to the minimum detectable signal.

In figure 3-12, it was difficult to see the effects of V_{CE} on the input noise. By plotting a subset of the same data on a linear scale, it is evident that V_{CE} varies directly with input noise, as stated in section 3.2.7. Also, the relative influence of I_C is much greater than that of V_{CE}. This result holds for the MDS, but only the input noise is shown here, in Figure 5-1.

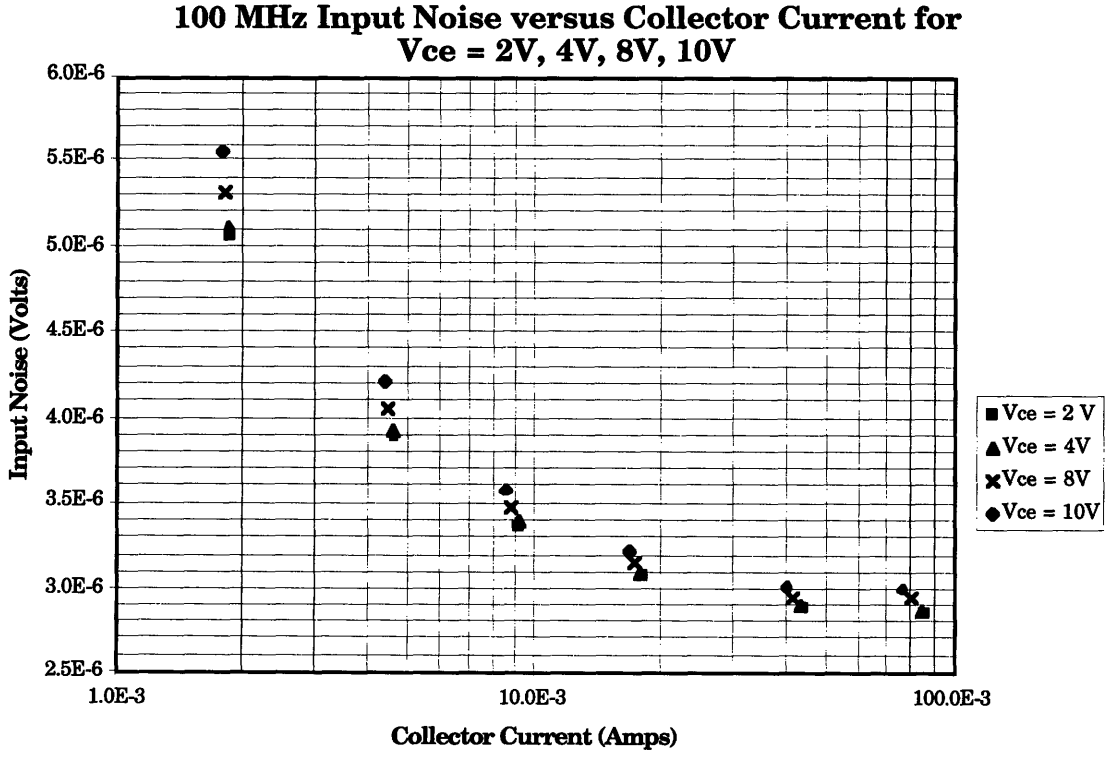

Figure 5-1: Comparison of I_C and V_{CE} effects on input noise

The effects of collector current and collector to emitter voltage on noise performance were confirmed in the laboratory. While there was a general correlation between HSPICE and MATLAB calculations as compared to the laboratory results, the noise measurements were consistently, noticeably higher.

There are a few possible sources of error between predicted and observed performance. The actual transistor's parameters may be worse than expected, and the circuit may require more shielding from ambient noise. If the circuit is not adequately shielded from the ambient noise, this could skew noise measurements. Different shielding techniques should be tested to see which is the most appropriate in this case. Also, the measurement techniques used here may give rise to erroneous data. Many calculations, especially the noise figure, were performed based on the data taken from lab using the configurations specified in Appendix H. A noise figure meter should be used to better account for the actual input noise.

A future study should also be performed on the variance of transistor parameters and their effects on noise performance. This was not taken into consideration here but a preliminary temperature and current gain, β, study was performed. The results, as shown in Appendix C, indicate that the design is temperature and β insensitive. This conclusion is based solely on HSPICE and MATLAB data and can be misleading without any data in from the laboratory to confirm it.

In addition to transistor parameter sensitivity, the dependence of the noise performance on the lower 3-dB frequency of the amplifier should

studied. This was not considered in this study however, the noise equations derived in Appendix B suggests that decreasing the noise bandwidth will decrease the MDS of the amplifier.

Appendix A

NOTATION

The Notation used in this document are governed by the these three rules:

1. External components, DC currents and DC voltages have upper-case symbols with upper-case subscripts.
2. Hybrid-pi parameters are expressed by lower-case symbols with lower-case subscripts.
3. Voltage gain, noise voltages and noise currents are expressed with upper-case symbols with lowercase subscripts.

A_V	Amplifier voltage gain transfer function
β	Transistor base-collector current gain
c_μ	Hybrid-pi model base-collector capacitor in Farads
c_π	Hybrid-pi model base-emitter capacitor in Farads
C_S	Source capacitance in Farads
E_b	Base resistance thermal noise in rms $V/Hz^{0.5}$
E_o	Total output noise voltage in rms $V/Hz^{0.5}$
E_{ob}	Output noise voltage due to base resistance noise in rms $V/Hz^{0.5}$
E_{or1}	Output noise voltage due to biasing resistance noise in rms $V/Hz^{0.5}$
E_{or2}	Output noise voltage due to biasing resistance noise in rms $V/Hz^{0.5}$
E_{orl}	Output noise voltage due to load resistance noise in rms $V/Hz^{0.5}$
E_{osb}	Output noise voltage due to base shot noise in rms $A/Hz^{0.5}$
E_{osc}	Output noise voltage due to collector shot noise in rms $A/Hz^{0.5}$
E_b	Base resistance thermal noise in rms $V/Hz^{0.5}$
E_{sb}	Base current shot noise in rms $A/Hz^{0.5}$
E_{sc}	Collector current noise in rms $A/Hz^{0.5}$
E_{r1}	Base biasing resistance thermal noise in rms $V/Hz^{0.5}$
E_{r2}	Base biasing resistance thermal noise in rms $V/Hz^{0.5}$
E_{rl}	Load resistance thermal noise in rms $V/Hz^{0.5}$
E_{mds}	Minimum detectable signal in rms $V/Hz^{0.5}$
E_{th}	Thermal Noise source in rms $V/Hz^{0.5}$
f	Frequency in Hertz
f_L	Flicker noise corner frequency in Hertz
Δf	Noise power bandwidth in Hertz
I	DC current in Amps
I_1	DC current flowing through R_1 in Amps
I_B	DC operating point base current in Amps
I_C	DC operating point collector current in Amps
I_b	Base current shot noise source in rms $A/Hz^{0.5}$
I_c	Collector current shot noise source in $A/Hz^{0.5}$
I_{sh}	Shot noise source in $A/Hz^{0.5}$

k	Boltzman's constant, 1.38 x 10^{-23} J/K
NF	Noise figure in decibels
q	Electron charge, 1.6 x 10^{-19} C
R_1	Base biasing resistor in Ohms
R_2	Base biasing resistor in Ohms
R_E	Emitter degeneration resistor in Ohms
R_L	Load resistor in Ohms
r_b	Hybrid-pi model base resistance in Ohms
r_π	Hybrid-pi model base-emitter resistance in Ohms
r_o	Hybrid-pi model base-emitter resistance in Ohms
S/N	Signal to noise ratio
T	Operating temperature in Kelvin
V_{BE}	Transistor base-emitter on voltage in Volts
V_{CE}	Transistor collector-emitter voltage in Volts
V_{pp}	Voltage swing in Volts peak-to-peak
V_{RL}	Voltage drop across R_L in Volts
V_T	Room temperature thermal voltage, 0.025 V
Z_S	Complex source impedance $(2\pi jfC_S)^{-1}$
z_π	Hybrid-pi model base-emitter impedance $r_\pi/(2\pi jfc_\pi r_\pi + 1)^{-1}$
z_μ	Hybrid-pi model base-collector impedance $(2\pi jfc_\mu)^{-1}$

Appendix B

NOISE EQUATIONS

Appendix B.1 Derivation of the small signal gain of a transistor amplifier

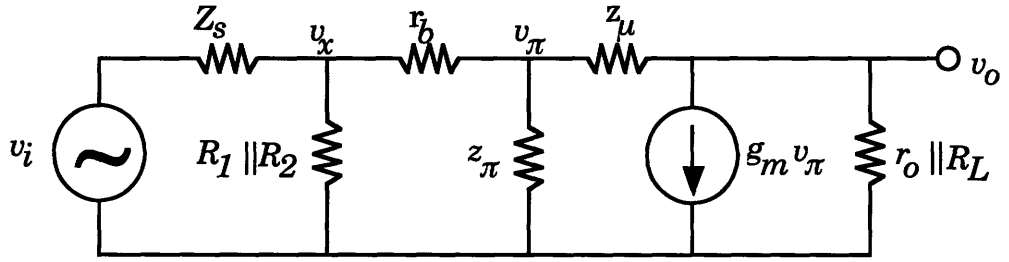

Figure B-1: Hybrid-pi model for a common emitter amplifier

Above is the small signal hybrid-π model for a common emitter amplifier, including all complex impedances, parasitic elements and the series source impedance.

Z_S = complex source impedance, $= R_S + \frac{1}{j2\pi f C_S}$

g_m = Hybrid-π model transconductance in mhos

R_1,R_2 = Base biasing resistors

r_b = Base contact resistance

Z_π = base to emitter complex impedance = $\frac{r_\pi}{j2\pi f C_\pi r_\pi + 1}$

Z_μ = base to collector complex impedance = $\frac{1}{j2\pi f C_\mu}$

R_L = load resistors

G_S = total parallel source impedance = $\frac{1}{R_1} + \frac{1}{R_2} + \frac{1}{Z_S}$

r_O = small signal output resistance

The amplifier voltage gain is derived from the following three KCL equations:

1. $$\frac{-v_O}{r_O \,||\, R_L} = g_m v_\pi + \frac{v_O - v_\pi}{z_\mu}$$

2. $$\frac{v_X - v_\pi}{r_b} + \frac{v_O - v_\pi}{z_\mu} = \frac{v_\pi}{z_\pi}$$

3. $$\frac{v_i - v_X}{Z_S} = \frac{v_X}{R_1} + \frac{v_X}{R_2} + \frac{v_X - v_\pi}{r_b}$$

Eliminating v_X, and v_π from the above equations yields:

$$A_V = \frac{-\left(g_m - \frac{1}{z_\mu}\right)\frac{1}{Z_S} R_L}{\left(1+\frac{R_L}{r_O}\right)\left[\left(\frac{1}{z_\pi}+\frac{1}{z_\mu}\right)(G_S r_b + 1) + G_S\right] + \frac{R_L}{z_\mu}\left[(G_S r_b + 1)\left(g_m + \frac{1}{z_\pi}\right) + G_S\right]}$$

Note that for infinite z_μ, R_1, R_2 & r_O, zero Z_S and r_b, the above equation reduces to $A_V = - g_m R_L$.

Appendix B.2 Derivation of the Minimum Detectable Signal

The small signal model for the amplifier including all noise sources is shown below.

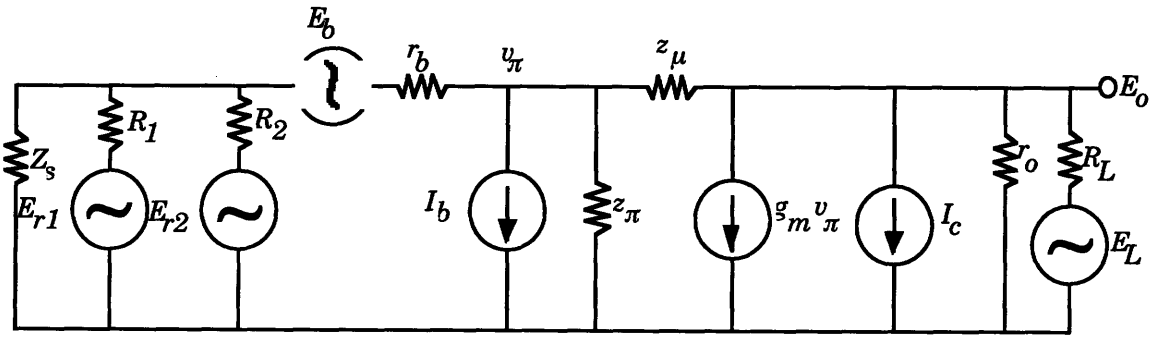

Figure B-2: Hybrid-pi model with noise sources

In order to calculate the minimum detectable input signal, the noise contributed to the output of the amplifier will be calculated for each noise source independently then the sum of all noise sources will be divided by the voltage gain of the amplifier.

B.2.1 Base biasing resistors thermal noise

$$E_{or1} = E_{r1}A_V \frac{Z_S}{R_1} \Rightarrow E_{or1}^2 = E_{r1}^2 A_V^2 \frac{Z_S^2}{R_1^2} = \frac{4kT}{R_1} A_V^2 Z_S^2$$

$$E_{or2} = E_{r2}A_V \frac{Z_S}{R_2} \Rightarrow E_{or2}^2 = E_{r2}^2 A_V^2 \frac{Z_S^2}{R_2^2} = \frac{4kT}{R_2} A_V^2 Z_S^2$$

where

T = Operating temperature in Kelvin

k = Boltzman's constant, 1.38 x 10^{23} J/K

B.2.2 Base resistance thermal noise

$$E_{ob} = -\frac{G_S\left(g_m - \frac{1}{z_\mu}\right)}{\left[\frac{R_L}{z_\mu}\left(g_m + \frac{1}{z_\pi}\right)(G_S r_b + 1) + G_S\right] + \left(1 + \frac{R_L}{r_O}\right)\left[\left(\frac{1}{z_\mu} + \frac{1}{z_\pi}\right)(G_S r_b + 1) + G_S\right]} E_b = G_S Z_S A_V$$

$$E_{ob}^2 = E_b^2 Z_S^2 G_S^2 A_V^2 = 4kTr_b Z_S^2 G_S^2 A_V^2$$

B.2.3 Base current shot noise

$$E_{osb} = -\frac{(G_S r_b + 1)R_L\left(g_m - \frac{1}{z_\mu}\right)I_b}{\left[\frac{R_L}{z_\mu}\left(g_m + \frac{1}{z_\pi}\right)(G_S r_b + 1) + G_S\right] + \left(1 + \frac{R_L}{r_O}\right)\left[\left(\frac{1}{z_\mu} + \frac{1}{z_\pi}\right)(G_S r_b + 1) + G_S\right]}$$

$$= A_V Z_S (G_S r_b + 1) I_b$$

$$E_{osb}^2 = I_b^2 Z_S^2 (G_S r_b + 1)^2 A_V^2 = 2qI_B Z_S^2 (G_S r_b + 1)^2 A_V^2$$

where

I_B = DC operating point current in amps

q = electron charge, 1.6 x10^{-19} C

B.2.4 Collector current shot noise

$$E_{osc} = \frac{\left[\left(\frac{1}{z_\mu} + \frac{1}{z_\pi}\right)(G_S r_b + 1) + G_S\right]R_L I_c}{\left[\frac{R_L}{z_\mu}\left(g_m + \frac{1}{z_\pi}\right)(G_S r_b + 1) + G_S\right] + \left(1 + \frac{R_L}{r_O}\right)\left[\left(\frac{1}{z_\mu} + \frac{1}{z_\pi}\right)(G_S r_b + 1) + G_S\right]}$$

$$E_{osc}^2 = I_c^2 Z_S^2 \left(\frac{(G_S r_b + 1)\left(\frac{1}{z_\pi} + \frac{1}{z_\mu}\right) + G_S}{g_m - \frac{1}{z_\mu}}\right)^2 A_V^2 = 2qI_c Z_S^2 \left(\frac{(G_S r_b + 1)\left(\frac{1}{z_\pi} + \frac{1}{z_\mu}\right) + G_S}{g_m - \frac{1}{z_\mu}}\right)^2 A_V^2$$

where

I_c = DC operating point collector current

B.2.5 Load resistor thermal noise

$$E_{ol} = \frac{\left[\left(\frac{1}{z_\mu}+\frac{1}{z_\pi}\right)\left(G_S r_b + 1\right) + G_S\right] E_l}{\left[\frac{R_L}{z_\mu}\left(g_m + \frac{1}{z_\pi}\right)\left(G_S r_b + 1\right) + G_S\right] + \left(1 + \frac{R_L}{r_O}\right)\left[\left(\frac{1}{z_\mu}+\frac{1}{z_\pi}\right)\left(G_S r_b + 1\right) + G_S\right]}$$

$$E_{ol}^2 = \frac{E_L^2}{R_L^2} Z_S^2 \left(\frac{\left(G_S r_b + 1\right)\left(\frac{1}{z_\pi}+\frac{1}{z_\mu}\right) + G_S}{g_m - \frac{1}{z_\mu}} \right)^2 A_V^2 = \frac{4kT}{R_L} Z_S^2 \left(\frac{\left(G_S r_b + 1\right)\left(\frac{1}{z_\pi}+\frac{1}{z_\mu}\right) + G_S}{g_m - \frac{1}{z_\mu}} \right)^2 A_V^2$$

B.2.6 Minimum detectable signal

The minimum detectable signal can be derived by adding all of the aforementioned noise components and dividing by the square of the voltage gain.

$$E_o^2 = E_{or1}^2 + E_{or2}^2 + E_{ob}^2 + E_{osb}^2 + E_{osc}^2 + E_{ol}^2 = A_V^2 E_{mds}^2$$

$$E_{mds}^2 = \frac{4kT}{R_1} Z_s^2 + \frac{4kT}{R_2} Z_s^2 + 4kTr_b Z_s^2 G_s^2 + 2qI_B Z_s^2 \left(G_s r_b + 1\right)^2 +$$

$$2qI_c Z_s^2 \left(\frac{\left(G_s r_b + 1\right)\left(\frac{1}{z_\pi}+\frac{1}{z_\mu}\right) + G_s}{g_m - \frac{1}{z_\mu}} \right)^2 + \frac{4kT}{R_L} Z_s^2 \left(\frac{\left(G_s r_b + 1\right)\left(\frac{1}{z_\pi}+\frac{1}{z_\mu}\right) + G_s}{g_m - \frac{1}{z_\mu}} \right)^2$$

Appendix C

SIMULATION ANALYSIS

Both HSPICE and MATLAB were used in order to analyze the performance of the circuit. HSPICE was used to determine the input noise of the circuit while MATLAB was used to calculate the minimum detectable signal and its components.

To determine the operating point of the amplifier that maximizes performance from a minimum detectable signal point of view, the bandwidth and the gain of the amplifier were held constant. The collector current was swept over a range from 10μA to 100 mA and the equations predicting the gain and resistor values for each bias point are presented below.

C.1 Biasing

As a starting point, 1 V was dropped across the load resistor, the transistor, and the emitter resistor. The resistor values can be found by $R_E = R_L = \frac{1}{I_C}$.

For this configuration, the base will be biased at $1+V_{BE}$ Volts. To minimize the error caused bias I_B, I_1 was set equal to I_C. Assuming that V_{BE} is 0.6V for this particular configuration, the voltage dropped across R_1 and R_2 is 1.4V and 1.6V respectively. Therefore, the base biasing resistors are governed by the following equations:

$$R_1 = \frac{1.4}{I_C}$$

$$R_2 = \frac{1.6}{I_C}$$

C.2 Gain

For a common emitter amplifier, the voltage gain is the product of the transconductance and the load resistor. This can be expressed as

$$A_v = g_m R_L = \frac{I_C R_L}{V_T} = \frac{V_{RL}}{V_T}$$

where V_{RL} is the voltage drop across the load resistor. For the previously mentioned configuration where V_{RL} is 1 V, the gain is 40.

C.3 Frequency Analysis (Short Circuit Time Constants)

The 3-dB bandwidth of the amplifier is determined by the load capacitor of the transistor of the common emitter but the low frequency 3-dB point is determined C_{in} and C_E. This frequency is set between 1 - 10 kHz by the following equation

$$f_l = \frac{1}{2\pi(R_S + R_1 \| R_2 \| (r_b + r_\pi))C_{in}} + \frac{1}{2\pi(R_E \| \frac{((R_S \| R_1 \| R_2) + r_\pi + r_b)}{\beta + 1} C_E}.$$

C.4 Second Order Effects

The performance of this amplifier was measured with respect to variations in β, which ranges from 50 to 300 for the NE856 transistor, and temperature variations. The results do not vary significantly.

C.4.1 ß Variations

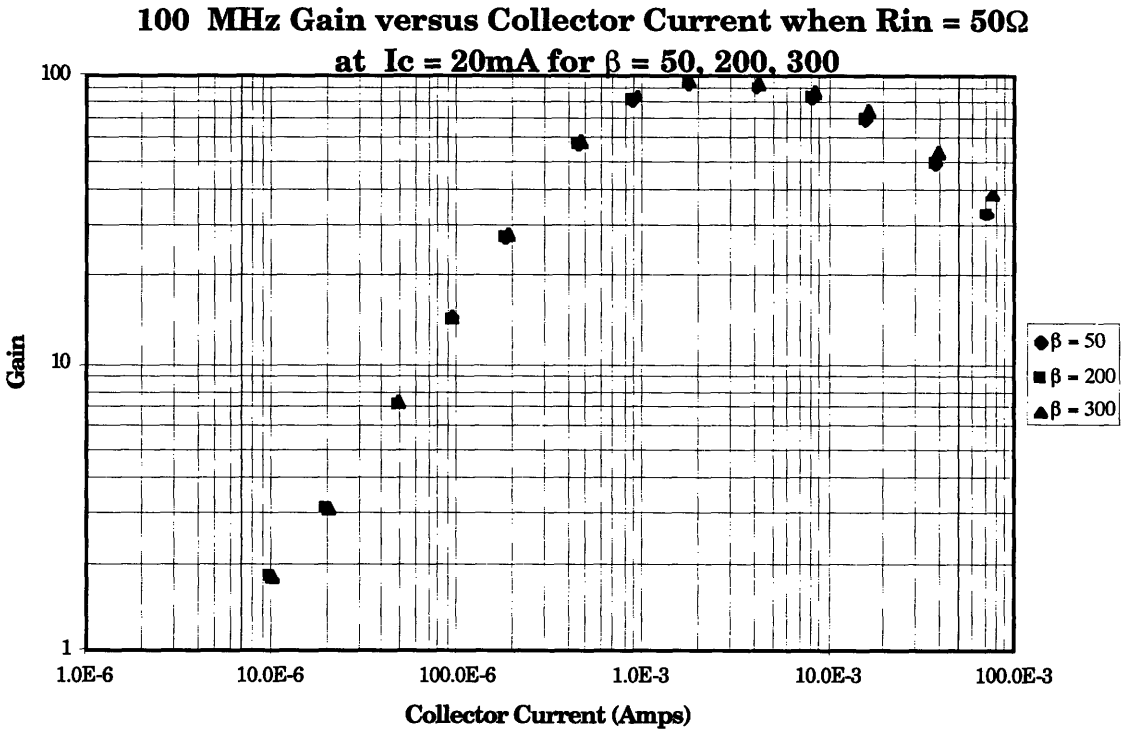

Figure C-1: 100 MHz gain versus collector current when β = 50, 200, 300

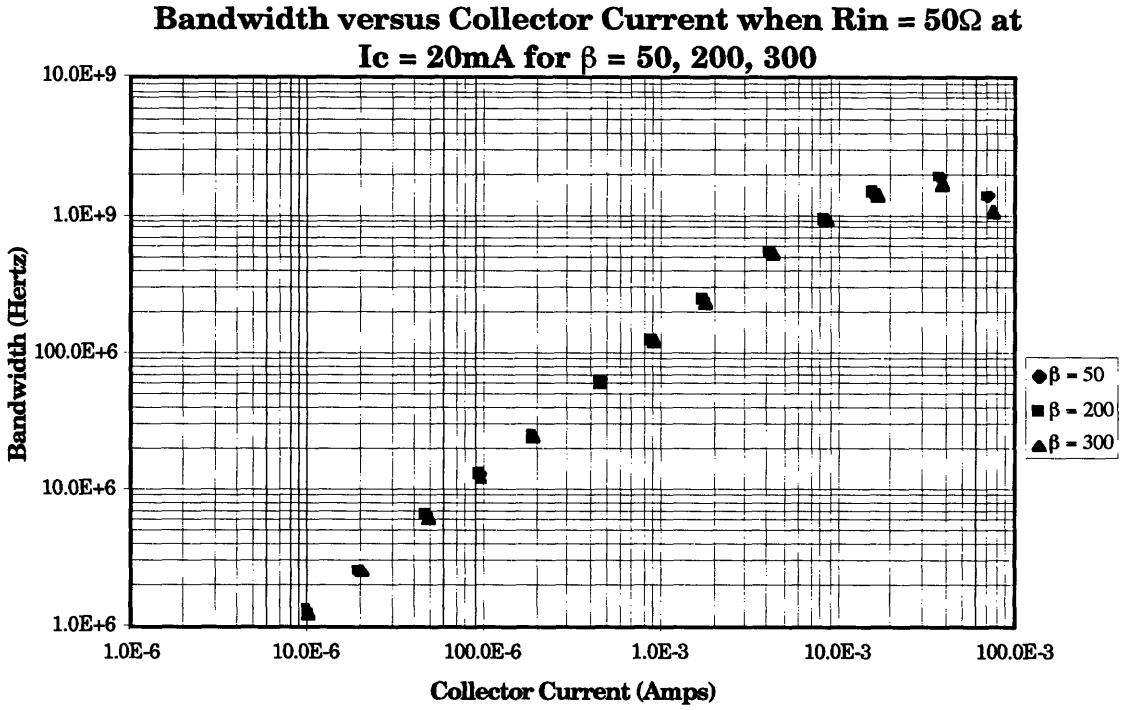

Figure C-2: 3-dB bandwidth versus collector current for β = 50, 200, 300

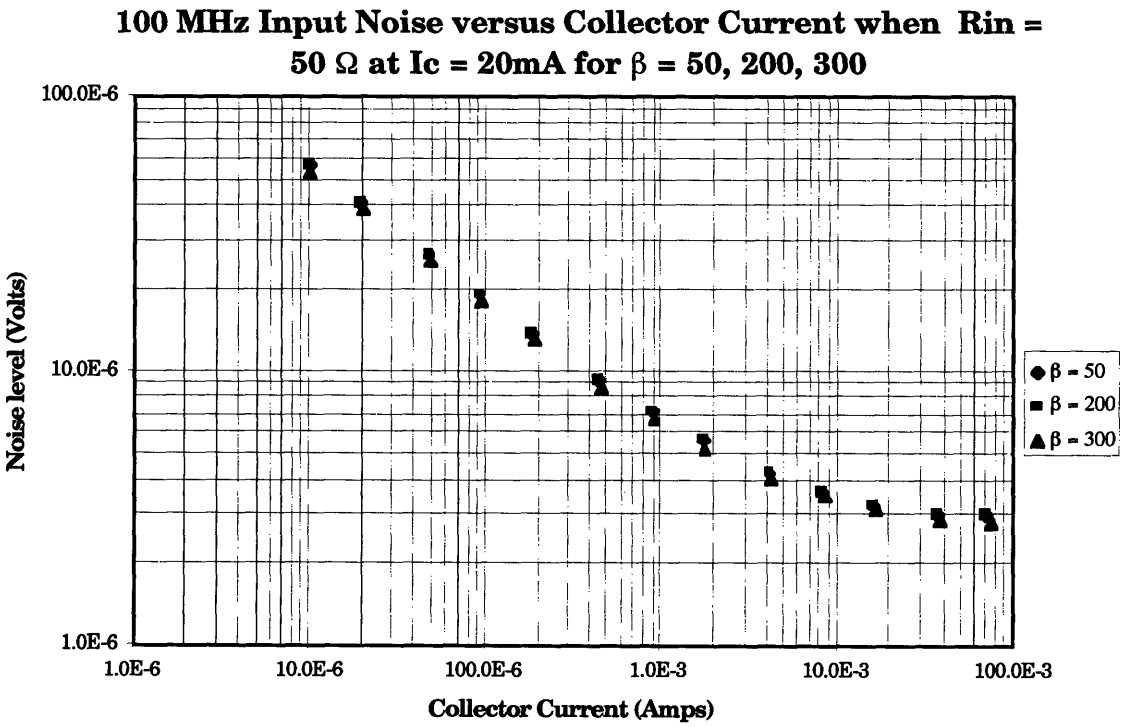

Figure C-3: 100 MHz input noise versus collector current for β = 50, 200, 300

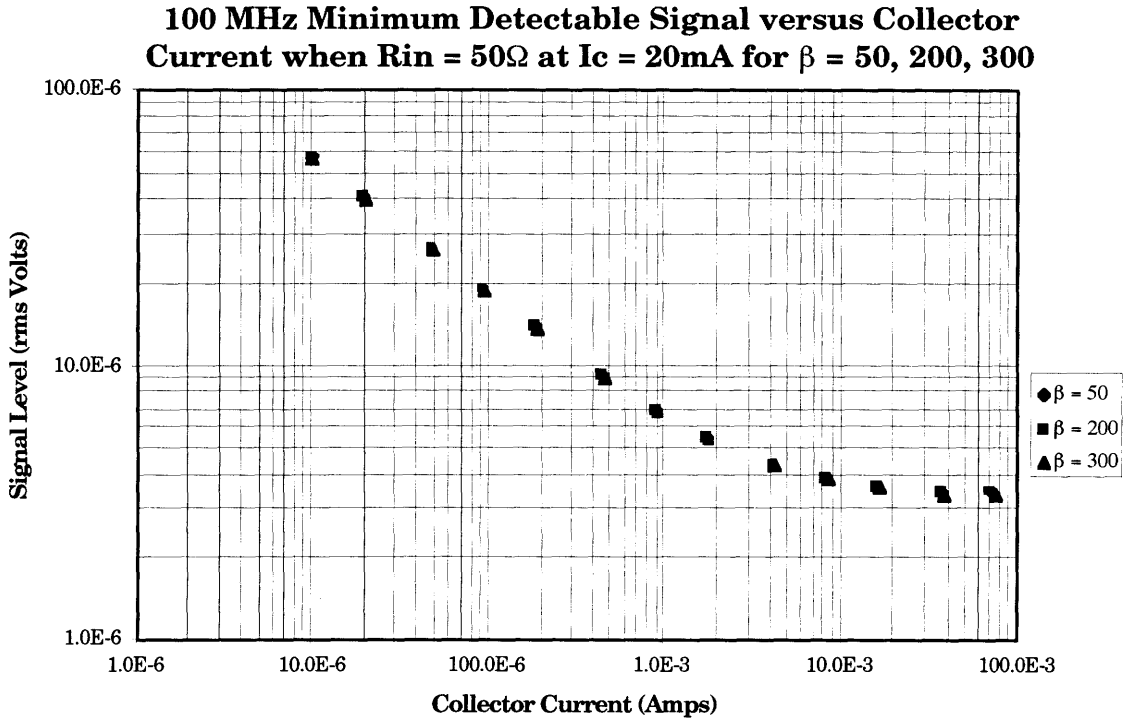

Figure C-4: 100 MHz MDS versus collector current for β = 50, 200, 300

C.4.2 Temperature Variations

For a ±10°C temperature variation about room temperature, there is a negligible change in noise performance.

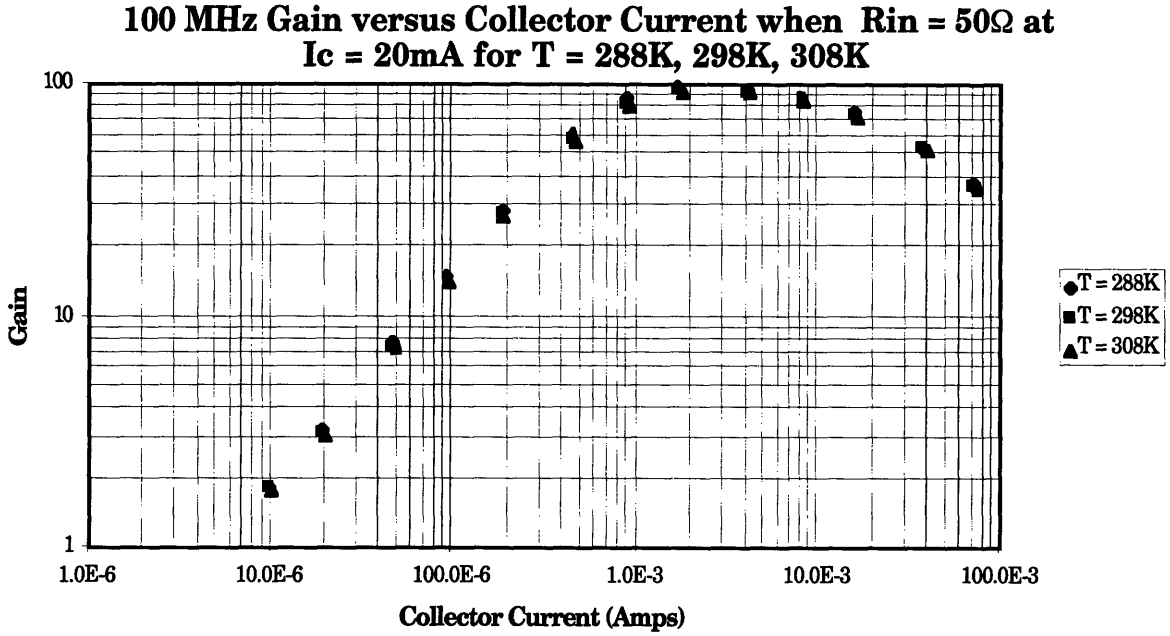

Figure C-5: 100 MHz gain versus collector current
when T = 15°C, 25°C, 35°C

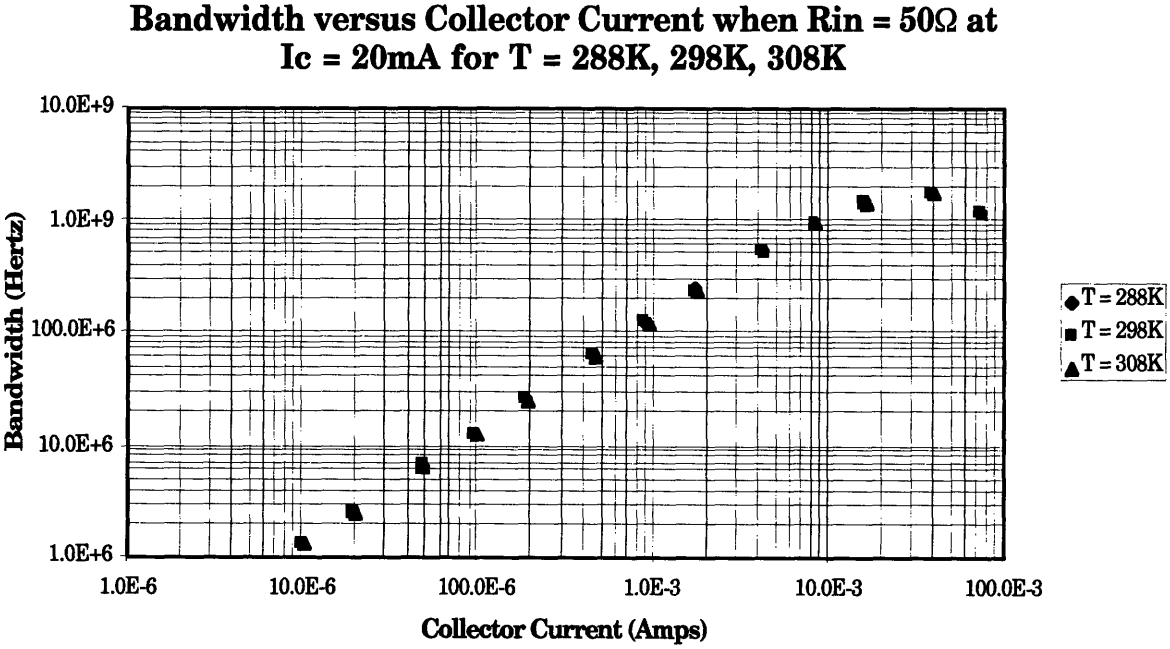

Figure C-6: 3-dB bandwidth versus collector current
when T = 15°C, 25°C, 35°C

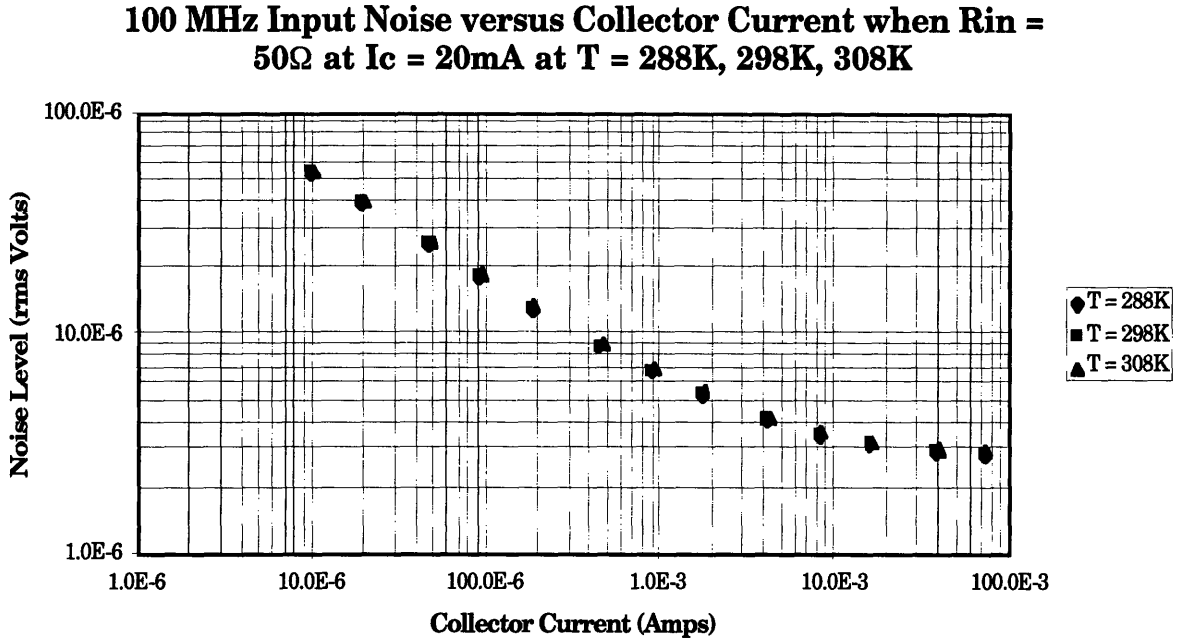

Figure C-7: 100 MHz input noise versus collector current when T = 15°C, 25°C, 35°C

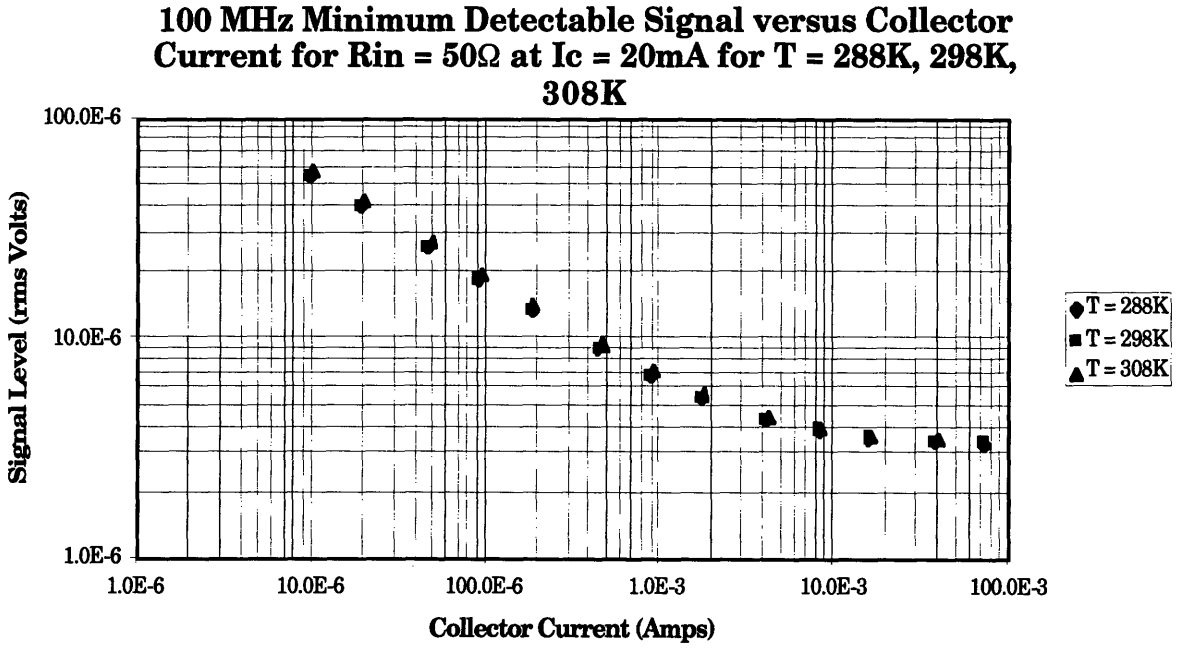

Figure C-8: 100 MHz MDS versus Collector Current when T = 15°C, 25°C, 35°C

Appendix D

HSPICE SIMULATIONS

D.1 NE856 HSPICE Model Parameters

spice name	value	spice name	value
IS	6E-16 A	MJE	0.33
BF	120	CJC	1.1 pF
NF	0.978	VJC	0.70 V
VAF	10.0 V	MJC	0.55
IKF	0.080 A	XCJC	0.3
ISE	32E-16 A	CJS	0 F
NE	1.93	VJS	0.750 V
BR	12	MJS	0
NR	0.991	FC	0.5
VAR	3.90 V	TF	10 ps
IKR	0.170 A	XTF	6
ISC	0.0 A	VTF	10
NC	2	ITF	0.2 A
RE	0.380 Ω	PTF	0 °
RB	4.16 Ω	TR	1 ns
RBM	3.6 Ω	EG	1.11 eV
IRB	1.96E-4 A	XTB	0
RC	2.0 Ω	XTI	3
CJE	2.8 pF	KF	0
VJE	1.3 V	AF	1

Table D-1: HSPICE NE856 model parameters

D.2 HSPICE Input File

NE856 common emitter

```
.MODEL NE856 NPN
+ IS=6.0e-16      BF=120.0    NF=0.978    VAF=10.0     IKF=0.080
+ ISE=32e-16      NE=1.93     BR=12.0     NR=0.991     VAR=3.90
+ IKR=0.170       ISC=0.0     NC=2.0      RE=0.380     RB=4.16
```

```
+ RBM=3.60      IRB=1.96e-4   RC=2.0      CJE=2.80e-12    VJE=1.30
+ MJE=0.50      CJC=1.10e-12  VJC=0.70    MJC=0.550       XCJC=0.30
+ CJS=0.0       VJS=0.750     MJS=0.0     FC=0.50         TF=10.0e-12
+ XTF=6.0       VTF=10.0      ITF=0.2     PTF=0.0         TR=1.0e-9
+ EG=1.11       XTB=0.0       XTI=3.0     KF=0.0          AF=1.0

vcc 5 0 9
vin 1 0 ac 1
rs 1 2 0
cs 2 3 Cs
r1 5 3 R1
r2 3 0 R2
q1 4 3 6 ne856
re 6 0 Re
ce 6 0 100e-6
rl 4 5 Rl
.op
.ac dec 10 1 4e9 DATA=bias
.DATA  bias
R1          R2          Re          Rl          Cs
643.5E+3    139.1E+3    100.0E+3    400.0E+3    2.0E-9
321.7E+3    69.6E+3     50.0E+3     200.0E+3    4.0E-9
128.7E+3    27.8E+3     20.0E+3     80.0E+3     10.0E-9
64.3E+3     13.9E+3     10.0E+3     40.0E+3     20.0E-9
32.2E+3     7.0E+3      5.0E+3      20.0E+3     40.0E-9
12.9E+3     2.8E+3      2.0E+3      8.0E+3      100.1E-9
6.4E+3      1.4E+3      1.0E+3      4.0E+3      200.2E-9
3.2E+3      695.7E+0    500.0E+0    2.0E+3 400.1E-9
1.3E+3      278.3E+0    200.0E+0    800.0E+0    998.9E-9
643.5E+0    139.1E+0    100.0E+0    400.0E+0    2.0E-6
321.7E+0    69.6E+0     50.0E+0     200.0E+0    4.0E-6
128.7E+0    27.8E+0     20.0E+0     80.0E+0     9.8E-6
64.3E+0     13.9E+0     10.0E+0     40.0E+0     19.2E-6
.enddata
.noise v(4) vin 10 DATA=bias
.options nomod nopage post
.measure ac vmax max v(4)
.measure ac f3db when v(4) = 'vmax*0.707' fall=1
.measure ac fl when v(4) = 'vmax*0.707' rise=1
.end
```

Appendix E

MATLAB SIMULATIONS

The following function was written for use in MATLAB to the calculate the minimum detetectable signal and its components.

```
function out = cemds();
%calculates mds
ic = exp((-6:.1:0)*log(10));
%constants
q = 1.6e-19;
k = 1.38e-23;
T = 298;
vt = 25e-3;

% ne856 model
rb = 4.16;
tf = 10e-12;
cje = 2.8e-12;
beta=120;
is = 6e-16;
va = 10;
cmu0 = 1.1e-12;

% small signal
ib = ic/beta;
gm = ic/vt;
rl = ic.^(-1);
re = ic.^(-1);
vbe = vt*log(ic/is);
r1 = 5*(2-vbe).*ic.^(-1);
r2 = 5*(1+vbe).*ic.^(-1);
rpi = beta*gm.^(-1);
rs=0;
cs = (2*pi*1000*(rs+(r1.^(-1)+r2.^(-1)+(rb+rpi).^(-1))).^(-1)).^(-1);
cpi = 2*cje+tf*gm;
cmu = cmu0/sqrt(1+.6/.4);
% noise components
r1r2n = 0;
rbn = 0;
ibn = 0;
icn = 0;
rln = 0;
noise_50 = 0;
% integration
fl = 1e3;
for f = exp((3.01:.01:7.8455)*log(10));
```

```
  zs = (rs+(2*pi*j*f.*cs).^(-1));
  zpi = rpi.*(2*pi*j*f.*cpi.*rpi+1).^(-1);
  zmu = (2*pi*j*f.*cmu.^(-1));
  gs = r1.^(-1)+r2.^(-1)+zs.^(-1);
   bigterm = ((gs.*rb+1).*(zmu.^(-1)+zpi.^(-1))+gs).*(gm-zmu.^(-1)).^(-1);
   %bigterm = ((gs.*rb+1).*(zpi.^(-1))+gs).*gm.^(-1);

  r1r2n = r1r2n + 4*k*T*(zs.^2).*(r1.^(-1)+r2.^(-1))*(f-fl);
  rbn = rbn + 4*k*T.*rb.*(zs.^2).*gs.^2*(f-fl);
  ibn = ibn + 2*q*ib.*(zs.^2).*(gs.*rb+1).^2*(f-fl);
  icn = icn + 2*q*ic.*zs.^2.*bigterm.^2*(f-fl);
   rln = rln + 4*k*T*(zs.^2).*rl.^(-1).*(bigterm.^2)*(f-fl);
  noise_50 = noise_50 + 4*k*T*50*(f-fl).*ic.*ic.^(-1);
 fl=f;
end
noise_50_ohm = sqrt(abs(noise_50));
mds = sqrt(abs(r1r2n)+abs(rbn)+abs(ibn)+abs(icn)+abs(rln));
nf = 10*log10((mds+noise_50_ohm).*(noise_50_ohm.^(-1)));
%mds = sqrt(abs(r1r2n+rbn+ibn+icn+rln))
loglog(ic,sqrt(abs(r1r2n)),'-',ic,sqrt(abs(rbn)),'--',...
ic,sqrt(abs(ibn)), ':', ic,sqrt(abs(icn)), '-.',...
ic,sqrt(abs(rln)),'.',ic,mds,'*',spiceic,inoise,'o',...
ic,sqrt(abs(noise_50)),'+');
title('Minimum Detectable Signal for the ne856')
xlabel('Collector Current (Amps)')
ylabel('Minimum Detectable Signal (rms Volts)')
legend('R1R2 noise','rb noise', 'Ib noise', 'Icnoise', 'Rl noise', 'MDS',' HSPICE Input
noise','50 Ohm noise')
figure
r1r2noise = sqrt(abs(r1r2n));
rbnoise = sqrt(abs(rbn));
ibnoise = sqrt(abs(ibn));
icnoise = sqrt(abs(icn));
rlnoise = sqrt(abs(rln));
fid = fopen('/mit/magic/noise_data','w');
num=0;
fprintf(fid,'ic\tR1R2 noise\trb noise\tIb noise\tIc noise\tRl noise\tMDS\tNF\n');
for num=1:61,
fprintf(fid,'%d\t%d\t%d\t%d\t%d\t%d\t%d\t%d\n',ic(num),          r1r2noise(nm),
rbnoise(num), ibnoise(num), icnoise(num), rlnoise(num), mds(num), nf(num));
end
```

Appendix F

OPEN CIRCUIT TIME CONSTANT ANALYSIS (OCTC)

Appendix F.1 OCTC for a Common Emitter Amplifier

To find a lower bound for the 3-dB bandwidth of an amplifier, the method open circuit time constants is used. The time constant associated with every capacitor in the circuit is computed and the inverse of the sum of time constants is the estimated 3-dB frequency.

This method of estimating a circuit's bandwidth is very powerful because it allows the designer to see which circuit parameters influence the bandwidth the most and also aids in "tuning" the bandwidth for a specific range, as is done in this case. A common emitter amplifier's small signal topology is

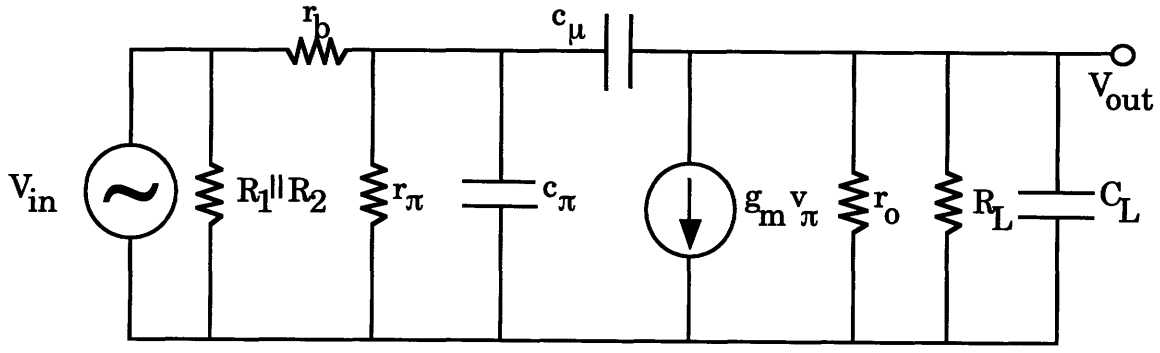

Figure F-1: Small signal model for the common emitter amplifier

To compute the individual time constant, the resistances "seen" by each capacitor must be found. $R_{\pi o}$, the OCTC resistance seen by c_π, is $r_\pi \,||\, (r_b + (R_1 \,||\, R_2))$.

For c_μ, we have $R_{\mu o} = (r_o \,||\, R_L) + (1 + g_m R_L)(r_\pi \,||\, r_b + (R_1 + R_2))$ as its open circuit time constant resistance.

If a load capacitor, C_L, is added to the circuit, it will see $r_o \,||\, R_L$. This capacitor is usually added in order to reduce the bandwidth, by setting its open circuit time constant much larger than the rest of the time constants.

The 3-dB frequency in Hertz, is given by $\frac{1}{2\pi \sum_j \tau_{jo}}$, where τ_{jo} is the time constant associated with each capacitor.

F.2 OCTC for a CE-CC Two-Stage Amplifier

A common-emitter-emitter-follower amplifier has the following small signal model:

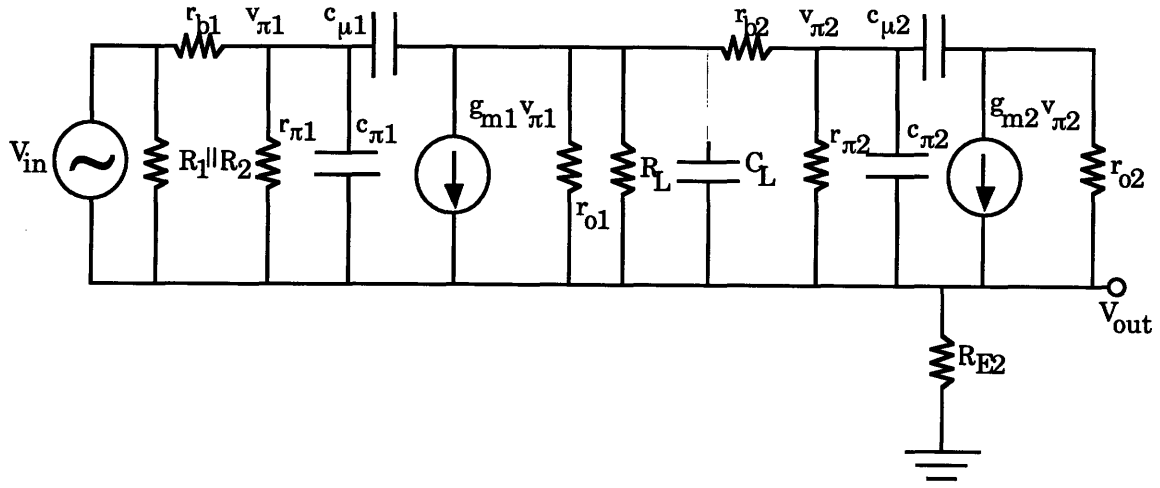

Figure F-2: Small signal model for the common emitter-common emitter follower

The open circuit resistances for this amplifier are:

$$R_{\pi o1} = r_{\pi 1} \| \left(r_{b1} + \left(R_1 \| R_2 \right) \right)$$

$$R_{\mu o1} = \left(r_{o1} \| R_L \| r_{\pi 2} \right) + \left(1 + g_{m1} R_L \right) \left(r_{\pi 1} \| \left(r_{b1} + \left(R_1 \| R_2 \right) \right) \right)$$

$$R_{\pi o2} = r_{\pi 2} \left\| \frac{\left(r_{o1} \| R_L \right) + r_{b2} + r_{\pi 2}}{1 + g_{m2} R_{E2}} \right.$$

$$R_{\mu o2} = \left(\left(R_L \| r_{o1} \right) + r_{b2} \right) \| \left(r_{\pi 2} + \left(\beta + 1 \right) R_{E2} \right)$$

Just as before, C_L is added to set the bandwidth by introducing a dominant pole. The resistance it sees, R_{lo} is $\left(R_L \| r_{o1} \right) \| \left(r_{b2} + \left(r_{\pi 2} + \left(\beta + 1 \right) R_{E2} \right) \right)$.

Appendix G

HSPICE NOISE MEASUREMENTS COMPARISON

Analytical noise calculations were compared with HSPICE results using the following impedance divider.

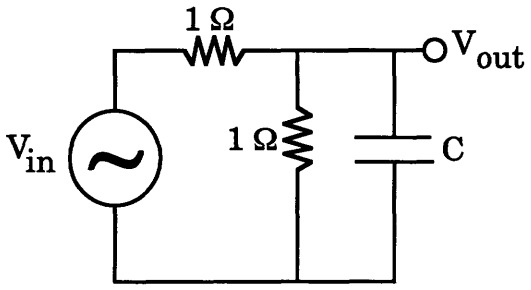

Figure G-1: Noise measurement comparison circuit

The transfer function is $\frac{V_{out}}{V_{in}} = \frac{1 \parallel \frac{1}{2\pi Cfj}}{1 + 1 \parallel \frac{1}{2\pi Cfj}}$. The noise model of the circuit is

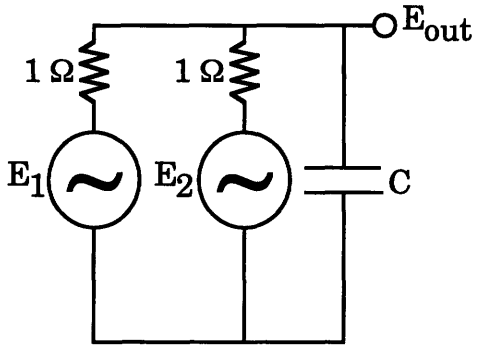

Figure G-2: Noise model of noise measurement comparison circuit

The noise output voltage is $E_{out}^2 = \left(\frac{1 \| \frac{1}{2\pi Cfj}}{1 + 1 \| \frac{1}{2\pi Cfj}} \right)^2 E_1^2 + \left(\frac{1 \| \frac{1}{2\pi Cfj}}{1 + 1 \| \frac{1}{2\pi Cfj}} \right)^2 E_2^2$.

Assuming a noiseless voltage source, the output noise will be due to the thermal noise of the resistors. If the capacitance is 1 μF and the noise power bandwidth is 1 kHz, HSPICE reports a noise output voltage of 2.8679 nV, while hand calculations give 2.8676 nV. This is a 0.01% discrepancy; henceforth, it is negligible.

Appendix H

BLOCK DIAGRAMS FOR NOISE MEASUREMENTS

Appendix H.1 Bandwidth and Gain Measurements

All gain and bandwidth measurements done in the laboratory are described in the block diagram:

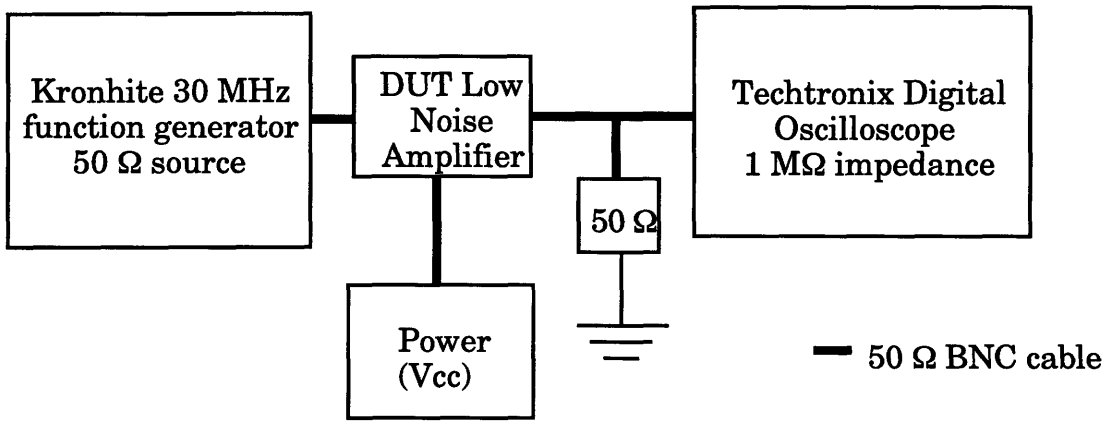

Figure H-1: Block diagram of gain and bandwidth measurements

Appendix H.2 Noise Figure Measurements

The noise figure measurements were taken with a Booton® ac true rms voltmeter in the following configuration:

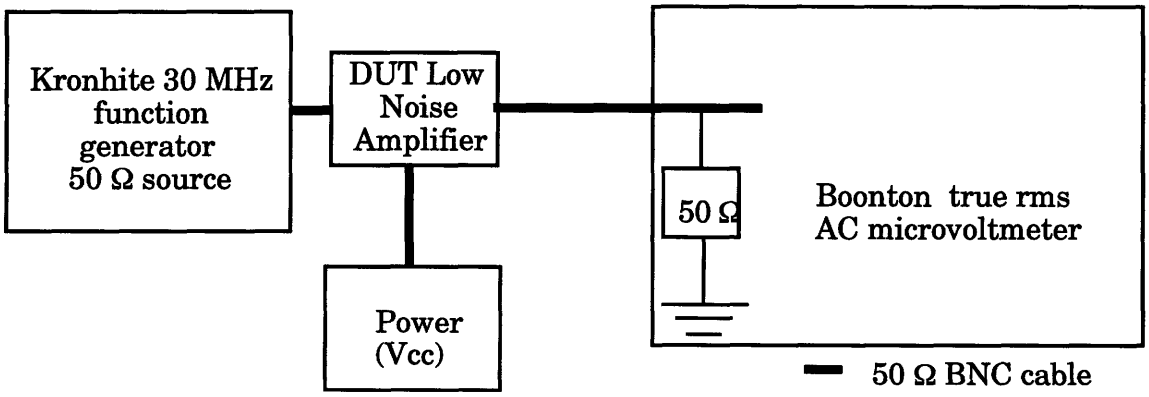

Figure H-2: Output noise and noise figure measurement block diagram

BIBLIOGRAPHY

1. P.R. Gray and R.G. Meyer. *Analysis and Design of Analog Integrated Circuits*.. Wiley, New York, 1977.
2. C.D Motchenbacher and F.C. Fitchen. *Low Noise Electronic Design.* Wiley, New York, 1973.
3. J.K. Hardy. *High Frequency Circuit Design.* Prentice-Hall, Reston, 1979.
4. Z. Wang. *Current-Mode Analog Integrated Circuits and Linearization Techniques in CMOS Technology.* Hartung-Gorre, Zurich, 1990.
5. C. Toumazou, F.J. Lidgely, and D.G. Haigh. *Analogue IC Design: The Current Mode Approach.* Peregrinus, London, 1990.
6. P.C.L. Yip. *High-Frequency Circuit Design and Measurements.* Chapman and Hall, New York, 1990.
7. J. Davidse. *Integration of Analogue Circuit Design.* Academy Press, London, 1979.
8. K. Lundberg. *Optimizing the Minimum Detectable Signal of Low-Noise Transistor Input Amplifiers.* MIT, Cambridge, 1992.